The Effect of Crystal Defects on the Performance of High-flux CZT X-ray Detectors

by

Niloofar Sadeghi
B.Sc., University of Tehran, 2012

A Thesis Submitted in Partial Fulfillment
of the Requirements for the Degree of

MASTER OF APPLIED SCIENCE

in the Department of Electrical and Computer Engineering

The Effect of Crystal Defects on the Performance of High-flux CZT X-ray Detectors

by

Niloofar Sadeghi
B.Sc., University of Tehran, 2012

Supervisory Committee

Dr. Tao Lu, Supervisor

(Department of Electrical and Computer Engineering)

Dr. Chris Papadopoulos, Departmental Member

(Department of Electrical and Computer Engineering)

Supervisory Committee

Dr. Tao Lu, Supervisor
(Department of Electrical and Computer Engineering)

Dr. Chris Papadopoulos, Departmental Member
(Department of Electrical and Computer Engineering)

ABSTRACT

Cadmium Zinc Telluride (CZT) has been one of the most promising semiconductor materials for many years. Due to its high atomic number, suitable band-gap energy and ability to function at room temperature, CdZnTe has become the material of choice to be used as a room temperature radiation detector for many applications in the fields of medical imaging, process monitoring and national security, where demands and specifications set by those applications require that these detectors can operate well at the extreme conditions while maintaining good resolution, high detection efficiency, good reliability and high throughput.

In most applications, detectors are exposed to high flux of X-ray radiation. One of the most common issues is the degradation of these detectors due to the presence of extended and point defects, which can act as traps for the charge carriers. This charge trapping causes the build-up of space charge and disturbing the electric field, resulting incomplete charge collection and signal formation of the detectors.

This thesis investigates the associated failure modes by identifying the types of defects that exist in the CZT crystal and studies their roles in the performance of X-ray radiation

detectors using in-house diagnostic tools. The results from different screening methods are compared and studied in order to find meaningful relationships and correlations that will help researchers to better understand the underlying physics and provide information and means for corrections and improvements of the crystal quality.

Table of Contents

List of Tables

List of Figures

Acknowledgments

I would like to thank my supervisor, Dr. Tao Lu, for all his guidance and patience during my project and supporting me in pursuing my favourite field of research. I would also like to express my sincere gratitude to my supervisors at Redlen Technologies, who helped me in each step of this work and made it happen, Dr. Saeid Taherion and Dr. Adam Densmore.

I would also like to thank Dr. Georgios Prekas especially, for being a great teacher, colleague and friend at the same time, from whom I learned a lot.

A big thanks to my colleagues and friends at Redlen and UVic who were of great support and help, Veeramani Perumal, Pramodha Marthandam, Jason McKenzie, Lindsay Burgess, Connor Neily, Ricky Lo, Wenyan Yu, Amin Cheraghi Shirazi and Serge Vincent.

At last, I like to express my gratitude to Redlen Company for giving me this great opportunity to work and learn in their progressive industry.

Dedication

To my father, my source of inspiration and support

my mother, my source of energy and unconditional kindness

my sister, the closest although she's so far away

and

my source of encouragement and love, Daniel Williams

1 Introduction

1.1 Semiconductor radiation detectors.

X-rays consist of high-energy photons that have a wide range of applications in medical radiography and airport security. [1-3] X-ray is not visible but it can be detected through their interaction with other materials. [4] X-ray detectors are designed to deliver information about the energy deposited by the incident radiation, its position or the radiation time. [5] There are three kinds of detectors commonly used for this purpose: Gas filled detectors, Scintillation detectors and semiconductor detectors, which is described below. [4]

- Gas filled detectors: Gas filled detectors consist of a metal chamber and a positively biased anode wire in between it. [4] X-ray beam interacts with the gas molecules inside the chamber and generates free electrons and positively ionized atoms. The free electrons are then absorbed to the anode and create signal.[6] These detectors occupy a large volume due to the low density, thus not practical in mobile applications.
- Scintillators: X-ray interacting with scintillators generates a pulse of light, which can be converted to an electric pulse and read through the proper electronic devices. [5] These detectors have a much smaller volume due to their higher density than the gas-filled detectors. However, in scintillators, a series of steps are needed take place to convert incident radiation into light and then the light into an electric signal. These multiple conversions can be very inefficient and so it requires high energy (in the order of hundred eVs) [5] to create electron-hole pairs. Consequently, the

number of information carriers per interaction is small, leading to large statistical fluctuations and low energy resolutions.

- Semiconductors: Similarly, X-ray interacting with semiconductor materials also results in the generation of electron-hole pairs. [4] These carriers can be guided through the material to the metal contacts under an electric field applied on the detector, generating an electric signal. [4] These detectors have similar feature size to scintillator detectors but produce a much larger number of information carriers per event because the energy required per information carrier is typically only a few eV rather than hundreds eV produced by the scintillator detectors [5]. Consequently, they do not have the same statistical limits as and can have much higher resolution than scintillator detectors.

Conventionally, silicon and germanium are the semiconductor materials used to fabricate radiation detectors due to their high density of atoms and high resolution. [5] Operational conditions of some of commonly used semiconductors are presented in Table 1. The growing needs for a detector applicable of working in room temperature and under high input X-ray irradiation lead researchers to use Cadmium Zinc Telluride (CZT) as the next generation of semiconductor materials for X-ray detector fabrication. [1-3, 7]

1.2 Advantages of CZT over other solid state materials

CZT has been the main semiconductor material for the fabrication of radiation detectors over the past two decades. The advantages of using CZT over other materials are evident from Table 1, where a brief comparison among different materials is illustrated. [8]

Table 1 - Comparison between different semiconductor materials used for radiation detection. [8]

	Si	**Ge**	**HgI_2**	**CdTe**	**CdZnTe**
Atomic Number	14	32	80, 53	48, 52	48, 30, 52
Density (g/cm^3)	2.33	5.32	6.4	6.06	6.06
Band gap (at Temperature, eV)	1.115 (300K) 1.165 (0K)	0.665 (300K) 0.746 (0K)	2.13	1.44	1.6 - 1.7
Ave. Energy/e-h pair (eV)	3.61	2.98	4.2	4.43	4.7
Electron Mobility (cm^2/Vs)	1350	3900	100	1100	1100
Hole Mobility (cm^2/Vs)	480	1800	4	100	100
Electron μτ Product (cm^2/V)	2.7×10^{-2}	0.72	10^{-4}	10^{-3}	10^{-3}
Hole μτ Product (cm^2/V)	9.6×10^{-3}	0.84	10^{-5}	5×10^{-5}	3×10^{-5}
Operating Temp. (K)	300	77	300	300	300

According to Table 1, CZT has a much higher atomic number than Si, which increases the effective interaction cross section between the atoms and incident photons, resulting a higher efficiency of generation of electron-hole pairs over the incident photons. A detailed discussion on light-matter interaction will be presented in chapter 2.

The higher operating temperature of CZT in comparison to Ge is also one of its other advantages. CZT detectors can operate in room temperature, while Ge detectors operate at a temperature below 77 K and require additional bulky cryogenic cooling apparatus. [8] This makes Ge detectors very expensive and not portable in contrast to the CZT counterpart. Among other properties that makes CZT an ideal choice for radiation detection in room temperature include, but not limited to [9]:

- Suitable band gap (about 1.55eV) that is large enough to provide high surface resistivity and low leakage currents (>10^9 Ω.cm) [9], but not too large to have a low absorption coefficient for the incident X-ray photons. [9] In addition, CZT is a direct band gap material. Therefore, there is no change in the momentum of electrons when transiting from the valance band to the conduction or vice versa, [4] leading to a better absorption of input photons due to the fact that input X-ray photon has almost zero momentum that could otherwise insufficient to conserve the momentum in in-direct band gap materials during the e-h pair generation. [6].
- Relatively high μτ product for electrons (≈1200 cm^2/Vs), where μ is the mobility of the carriers and τ is the carrier lifetimes and their product is an indicator of transport properties of material. This results in high charge collection efficiency by the electrons in the conduction band. [6] It is worth mentioning that holes in the valence band have low charge collection efficiency (≈100 cm^2/Vs) [2], causing incomplete hole collection, widening of photopeak and low spectrometer energy resolution. Some CZT sensor designs, such as Co-Planar Grid detectors (CPG) [10], were proposed to overcome this problem by eliminating the effect of holes in signal formation.

1.3 Current limitations of CZT as commercialized X-ray detector

To fabricate high flux, high resolution and room temperature CZT radiation detectors, high purity, defect-free material is desirable. This makes the corresponding crystal growth and fabrication processes challenging [11-13]. Typically, defects are introduced to the material during both the growth process and post processing such as annealing or during fabrication. Such defects can be classified in two major categories: extended defects and point defects.

[4] Extended defects are formed during the growth process. In general, extended defects can have the size as small as some micrometers to tens of milimiters [9] and their location and severity can be inspected using visual microscopy methods. [64] On the other hand, point defects are caused by impurities introduced to the material during the same process; acting as trapping centers for free carriers. [14] As point defects typically have a feature size of a single or multiple atoms [4, 9], they cannot be inspected visually. Therefore, analytical methods are commonly used to quantitatively and qualitatively identify them. Overall, both extended and point defects degrade the performance of the detectors and decrease the yield of material dramatically. [15] In particular, under high fluxes condition when high incoming irradiation and high density of carriers flowing through the detector, any impurity can distort the drift and collection of the carriers, resulting in severe field distortions and performance degradation. [9] Therefore, reducing the crystal defects is the major challenge in producing large volumes of commercial ready CZT detectors.

1.4 The goal of this thesis

In this work we study both extended and point defects in the CZT crystals. Different methods for screening these defects were used and the results were compared to detectors' performance in order to determine the impact of these defects on the yield of the CZT detectors.

The results in this thesis can be an important feedback to crystal growers and fabrication technicians in order to eliminate the defects to improve the quality of material, which will result in higher number of better performing detectors.

1.5 Thesis outline

The thesis structure is as follows:

Chapter 2 introduces the CZT material and its growth process, its working principles as a radiation detector, different types of defects in CZT crystal and their sources and finally the problems associated with these defects.

Chapter 3 provides the methods used for screening and evaluating the quality and performance of the detectors used in this study.

Chapter 4 includes the results of all the experiments using different spectroscopy methods followed by a discussion section, which relates and concludes the effect of different type of defects and operational conditions on the performance of detectors.

Chapter 5 provides a short summary and conclusion of the thesis.

2 Background

In this chapter, properties of CZT as a semiconductor material are investigated. This can help in understanding the mechanisms of CZT radiation detectors. Different growth methods of CZT and modifications to solve the major drawback of this material, which is defects present in the material, are introduced. After introducing the material, interaction of X-ray photons with the CZT atoms followed by signal formation and electronics needed to read this signal are studied. At the end of this chapter different types of defects present in the material and associated issues with them are introduced, which are the most important concern of this work.

2.1 CZT semiconductor material

2.1.1 CadmiumZincTelluride structure

CZT was first proposed as a suitable semiconductor material for radiation detection in late 1980s [14]. It is formed by alloying CadmiumTelluride (CdTe) and ZincTelluride (ZnTe) both have Zincblende structures. Consequently, CZT has a structure of a pair of interpenetrating face centered cubic (fcc) sub-lattices, which have an offset of a quarter of a unit cell body diagonal with a Cd or Zn atom being the center of one of the sub-lattices and Te atom the center of the other. [16] In general, the compound is expressed as $Cd_{1-x}Zn_xTe$ which implies that this alloy is basically made of CdTe, where Zn atoms have replaced Cd randomly for a mole fraction of x.

CdTe and ZnTe are both direct-bandgap material with a band-gap of around 1.4 eV and 2.2eV in room temperature, respectively. [17] Their compound, CZT, also has a direct-band gap of around 1.5eV-1.55eV depending on the Zn concentration. Figure 1 illustrates the schematic of a direct bandgap material. As the light-matter interaction follows the law

of momentum conservation, the transition of electrons from valance band to conduction band through photon absorption does not require excessive momentum change beyond that carries by the photon. This makes a direct bandgap material ideal for optical and radiation detection applications. In contrast, an indirect bandgap material generally requires the assist of third party particles for the electron-hole generation to occur. [18-21].

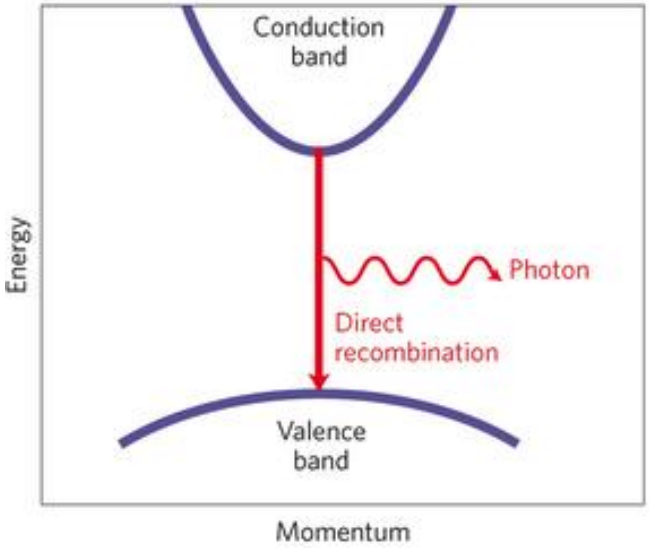

Figure 1 - Bandgap structure of a direct bandgap material.

2.1.2 Crystal growth process

As discussed earlier, despite the advantages of CZT over other semiconductor materials in fabrication of radiation detectors, low crystal quality and defects present in it are still barriers in commercializing large volume CZT radiation detectors. There are ongoing researches to improve the current crystal growth processes. [5, 22-31] Consequently, different methods for growing CZT crystals with continuing improvements are reported, which include Bridgman method [32-34], high-pressure Bridgman method [23-25], physical vapour transport method [35] and travelling heater method. [22] Despite of the advances, growing a perfect, defect and crack free crystal is still a goal yet to be achieved. As an illustration, some of the commonly used methods for CZT growth include:

- **Bridgman method:** In this method the crucible with a seed consisted of the same desired crystal, goes through a furnace with temperature above the crystal melting point. [36] The furnace can be vertical or horizontal. The crucible, the furnace or both can be moving. As the crucible exits the furnace very slowly, the melted crystal starts to solidify from the seed side and follow the structure of the seed resulting in a single crystal boule.
- **High pressure Bridgman (HPB) method:** In this method a pressure of 10-150 atm of an inert gas is present over the melt to reduce the loss of volatile components. [6] Despite the use of this inert gas, there is still problems such as cadmium loss (the component with highest vapour pressure component), which yields Te rich material. This will later result in having many Te inclusions and Te precipitate in the crystal and as the band-gap of Te is comparatively low (about 0.33eV), leading to a higher leakage current of the crystal.
- **Physical vapour transport (PVT):** This method is usually used for smaller boule sizes, but has a comparatively better quality in terms of extended defects. In this method CdTe and ZnTe poly-crystals are placed in a quartz growth chamber and by reaction between their vapours the CZT crystal is formed. Because of less contact with the containment and slightly lower temperature, the resulting crystal will be less contaminated and under less heat stress. This method can be used for both seeded and unseeded growth. An important factor of PVT is undercooling which is the temperature difference between the growing crystal and source materials. The higher the temperature difference, the faster the crystal will grow, but be less uniform. [27-29] Depending on the application and the quality requirement one can optimize the temperature.

- **Traveling heater method:** In this method, a Tellurium solution with Indium doping to compensate Cadmium loss during the growth and containing precise amount of Zinc, is used to grow high quality, high resistivity CZT single crystal. A narrow moving heater zone is present between the molten solution and solid crystal and the slower this heater area moves, the better quality crystal we will get. [31] A simple schematic of the process is shown in Figure 2. This method has proved to be a reliable method for high quality, defect-free CZT crystal growth and is the method currently used in Redlen Technologies.

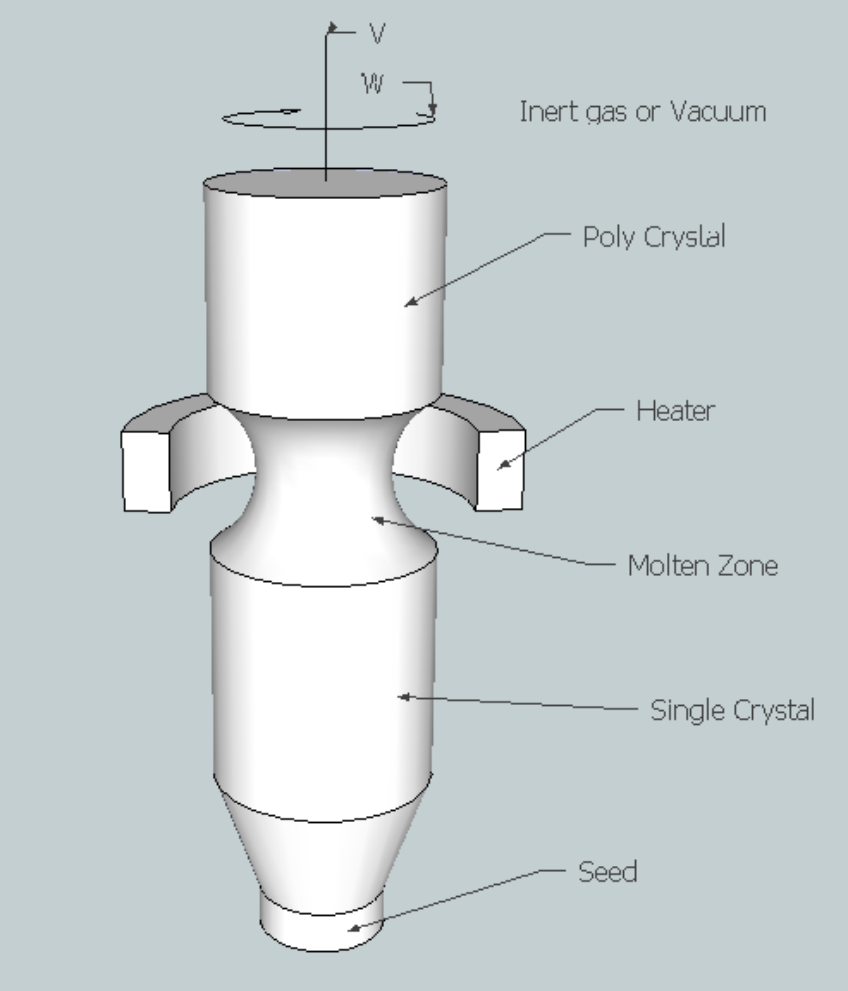

Figure 2 - Schematic of a travelling heater method system for CZT crystal growth. The heater moves along the crystal to create perfect crystal structure.

After resolving the growth issues and obtaining an acceptable crystal quality, the wafers go through the fabrication process. Details of the fabrication process of detectors are described below: metal contacts are deposited on the anode and cathode sides and surface is passivated to decrease the leakage current. The detectors are then tested under X-ray irradiation for their performance to be evaluated. In the following sections, the process of light interaction with material, generation of charge carriers, signal formation and methods to read the generated signal are discussed.

2.2 Interaction of radiation with matter

After the detectors are irradiated by the X-ray photons, the atoms go through an interaction with the photons. This interaction mainly consists of three major mechanisms: photoelectric absorption, Compton Scattering and pair production. [37] All these processes involve photon energy transfer, partially or completely, and with the photon being either disappeared or scattered with a significant angle. A brief description of each interaction comes below:

- **Photoelectric absorption:** In this process a photon goes through an interaction with an absorber atom. As a result the photon disappears completely and a high-energy photoelectron is ejected from one of the bound shells of the atom. Thus the energy of the photoelectron will be equal to the energy of the incident photon minus the binding energy of the electron. It should be noted that this interaction only happens with absorber atoms not free electrons. Equation (2.1) [5] gives an approximation of the probability of occurrence of photoelectric absorption:

$$P_{PE} \sim \frac{Z^4}{E^{3.5}} \tag{2.1}$$

  Where Z is the atomic number of the material and E is the energy of the incident beam. [4-5] Based on this equation we can see that the higher atomic number of CZT is in favour of photoelectric absorption process for comparatively low photon energies, which makes it ideal for X-ray detection applications.

- **Compton Scattering:** This process occurs between X-ray photons and an electron in an absorbing material. In this case, the incident photon is deflected at an angle with respect to its original direction and transfers a portion of its

energy to the electron, [4] which is known as “recoil electron” after incident. This portion of energy can be between zero to a large fraction of the original photon’s energy.

- **Pair production:** If the incident photon’s energy is twice the rest-mass energy of an electron (1.02 MeV), it is possible that pair generation occurs. [4] This interaction occurs in the coulomb field of a nucleus and the gamma or X-ray transfers all its energy, making an electron-positron pair instead. The energy exceeding the 1.02 MeV energy of the rest-mass energy will be divided between the electron and positron. As the positron transforms its energy to radiant energy, two lower energy photons are usually produced as the secondary products of this interaction.

Figure 3 illustrates the probability of each of the above three interactions for absorber atoms with different atomic numbers and for different energies of the incident radiation. τ, σ and κ represent the probability of photoelectric absorption, Compton scattering and pair production interaction occurrence, respectively. [4]

It can be observed that, photons with lower energy interact with material via the photoelectric absorption or Compton scattering mechanisms with an equal probability. In higher photon energies, Compton scattering and pair production are the dominant mechanisms. In all of the above interactions, the probability of the interactions increases with the atomic number of the material.

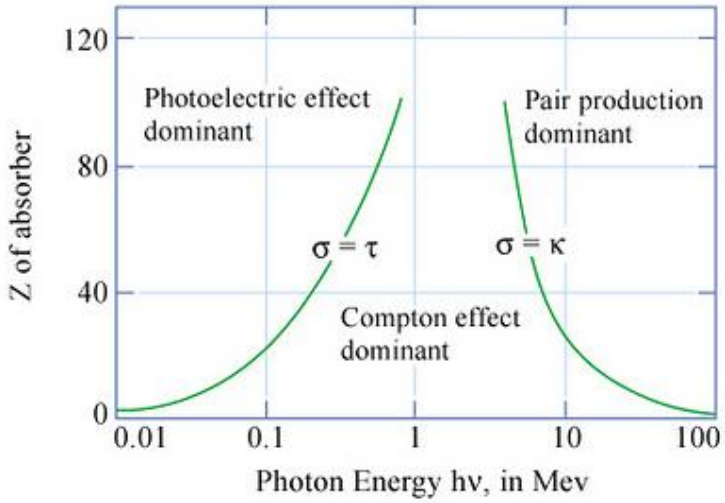

Figure 3 - Different types of light interaction with matter with respect to atomic number of the material and the incident photon energy. τ, σ and κ represent the probability of photoelectric absorption, Compton scattering and pair production interaction occurrence, respectively. [4]

2.3 Signal formation in CZT radiation detectors

2.3.1 Radiation detection mechanism in CZT detectors

The major light-matter interactions in the case of radiation sensing are photoelectric absorption and Compton scattering. [4, 37] After the incident photons interact with the CZT atoms with either of the mechanisms, relatively high-energy electrons are produced as a result of the interaction. The effect of these electrons is what needs to be sensed. In order to do so, a bias voltage is applied over the detectors to create an electric field between anode and cathode. [4-5] This electric field over the detector plays one of the main roles in charge transfer and hence sensing the incident light. [9] The high energy electrons generated by the X-ray photons travel a path along the electric field and on their way they generate phonons and electron-hole pairs before they come to rest. This process can create

relatively large clouds of low energy electrons and holes. For example for a 100keV electron the size of this cloud is approximately 20μm in diameter.[4-5]

These clouds of charge carriers then move towards either anode or cathode. Their drift velocity is dependant on the amplitude of the electric field. By having a stronger electric field we can have a faster and stronger charge collection. [5] A schematic of the charge created in the CZT material and its traveling direction are presented in Figure 4.

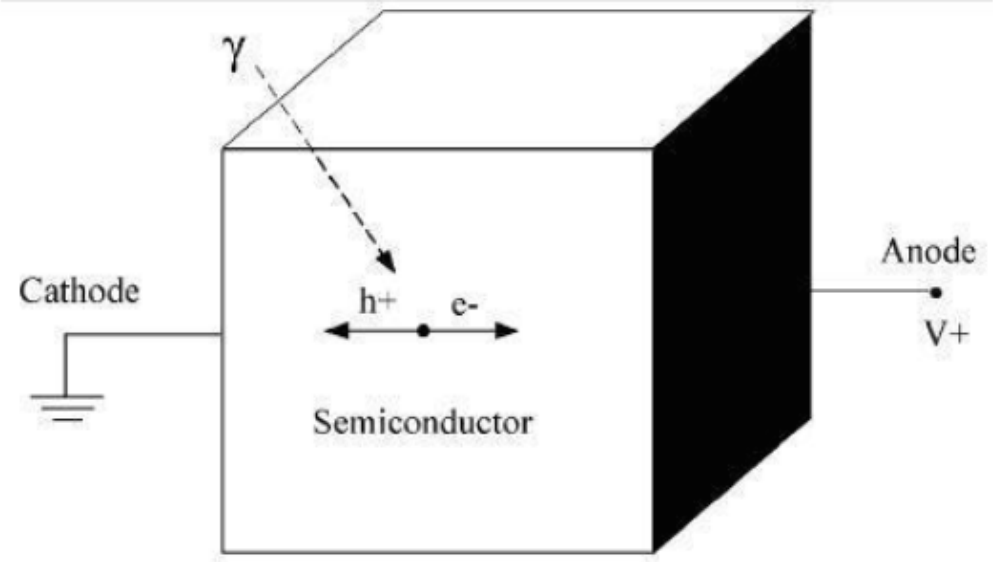

Figure 4 - Charge created by the incident gamma rays and the direction of electrons and holes transfer due to the electric field applied between anode and cathode. [38]

In more details, based on Ramo's theorem [39], a single charge q moving a distance dx in the direction of the electric field E, induces a charge dQ on either of the terminals of the detector.

$$V \cdot dQ = E \cdot q \cdot dx \tag{2.3}$$

Where V is the potential difference between the terminals and E=V/D and D is the detector's depth. By substituting them in the above equation we will have:

$$dQ = \frac{q \cdot dx}{D} \tag{2.4}$$

By writing the above equation for both electrons and holes and adding them to obtain the whole induced charge will equal to:

$$dQ = \frac{q \cdot dx_e}{D} + \frac{q \cdot dx_h}{D} = \frac{q}{D} \cdot (dx_e + dx_h) \quad (2.5)$$

So the total charge can be obtained by integrate along the path:

$$Q = \frac{q \cdot N_0}{D} \cdot (L_e + L_h) \quad (2.6)$$

Where N_0 is the total number of carriers and L_e and L_h are the minimum of drift lengths of electron or hole clouds and detector's depth, respectively. Drift lengths are defined as the distance that carriers travel before they are recombined. In an ideal case these drift lengths of electron and hole clouds should be much larger than the thickness of the detector, D, so that all the created charge will be sensed. [14]

In reality, due to trapping and other defects only a portion of the excess carrier generated reach the electrodes. This can be simply defined as the charge finally collected at the contacts divided by the charge created after the interaction with incident photons, known as charge collection efficiency (CCE) [5]:

$$CCE = \frac{Q}{Q_0} \cdot 100\% \quad (2.7)$$

Subsequently, the collected charge needs to be read through electronic circuits to make an analyzable data for the user.

2.3.2 Modes of operation

There are different methods of reading the output of the radiation detectors with different levels of complexity and each has their own advantages and disadvantages. Most of them use an application specific integrated circuit (ASIC) for the read out circuit with different designs. [40] The whole circuit is bump-bonded to the external pixel of the detectors by

indium balls or epoxy. [40] A picture of the ASIC circuit used for this study is displayed Figure 5.

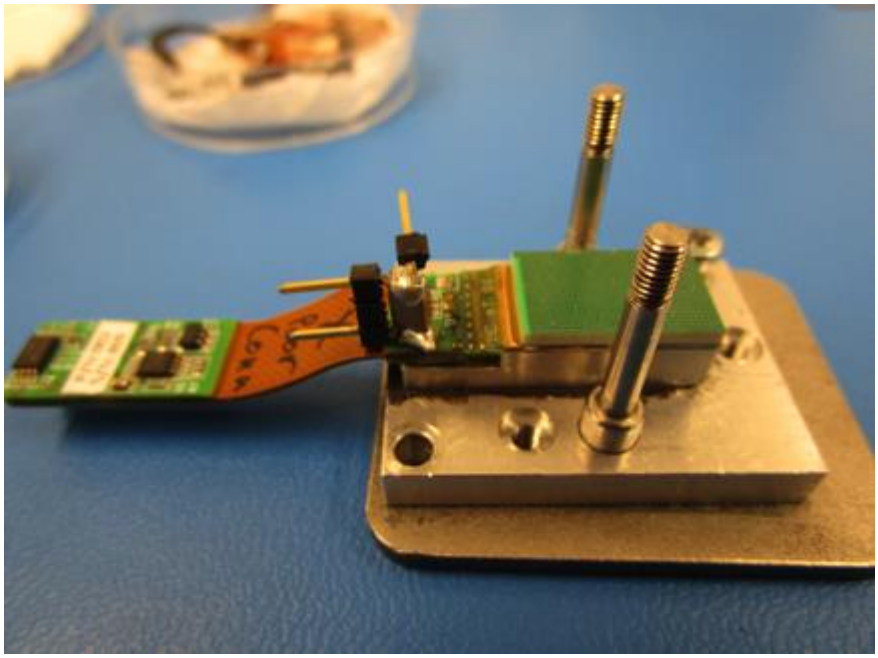

Figure 5 - The ASIC and bump-bonded connector. Detectors are aligned and secured in place on top of the connector and then will be placed in the X-ray tester.

Here we introduce two most important and common methods for radiation detectors read-out:

- **Charge integration mode:** In this mode the charge sensed by the radiation detector is integrated on an in-pixel capacitor to be read later. [40] The average charge is then calculated by the average event rate multiplied by charge produced by event. A sample of the read-out charge versus time is shown in Figure 6.

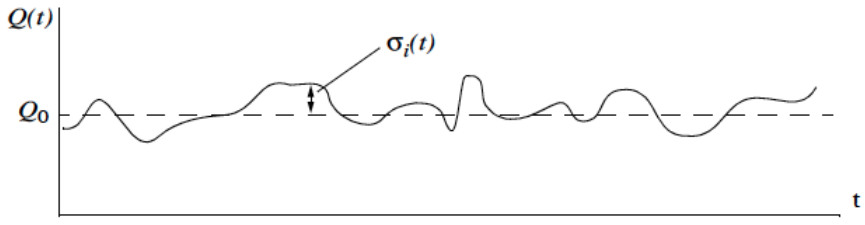

Figure 6 - Calculating the average charge read-out with charge integration mode. Final record will lose the detailed information about position and size of the peaks. [40]

Simple circuits used for this method and low levels of noise make it a cost effective, available mode for signal detection. [40-41] On the other hand, this does not store any information about energy and the timing of the incident irradiation. [41] It also does not have the enough sensitivity for low charges as it is stated as the average charges over a period of time that might be much greater than the actual minimum charge. [41] For all these reasons, this mode of operation is not the main mode of interest for high flux detectors.

- **Photon counting mode:** This mode of operation is the most interesting and also the most challenging mode for the researchers working especially with high flux detectors. [42] It has higher accuracy than charge integration mode but needs more complicated electronic circuits in order to operate. [40] In this method each individual quanta of radiation is counted, so it has very high sensitivity. [40] It also has a much lower limit for the minimum charge detected [40] and as the currents of the CZT detectors are very low, it is an important advantage over the charge integration mode. It is a faster mode of operation [40-41] and thus is more suitable to handle the fast response of the CZT detectors. More importantly, for being able to sense the correct peaks at correct energy thresholds of the X-ray

spectrum (also known as bins) we need information about each pulse heights and their timings that only photon counting method can provide. [40-41, 43] Figure 7 shows a schematic of a photon counting pixel read-out circuit. [43] The analogue voltage sensed turns into digital with respect to different thresholds specified with red and blue in the figure. The final counting is a result of summation of individual counts recorded and is what we see as the output count-rate of the detectors.

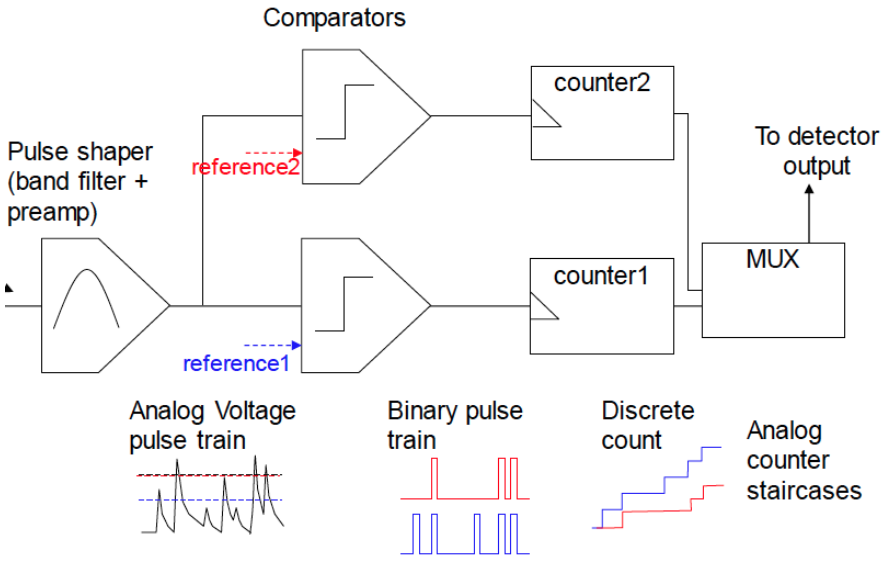

Figure 7 - The photon counting pixel circuit. Different thresholds for reading the output count-rate are noted by red and blue colors. [43]

We had an overview of the working principal of the CZT radiation detectors so far. In the next section we study different types of defects present in the CZT material and their impact on performance of the detectors.

2.4 Point defects

Point defects are referred to the defects in the size of single atoms caused during the process of crystal growth. They can be impurity atoms or vacancy of some atoms. These

defects are considered to be responsible for charge trapping and polarization phenomenon, leading to performance degradation of CZT detectors. [44-49] Carriers generated by X-ray illumination can be trapped by these defects, resulting in build-up of carriers and distortion in field distribution and causing performance degradation of the detectors. [42] These defects are in the size of single atoms and they cannot be inspected by visual microscopy methods. Therefore, analytical methods are needed to identify them. Some of the common point defects present in CZT crystals are introduced below, where there are still some that their sources are unidentified and under debate.

One of the common sources of point defects in CZT crystal is the impurity introduced to the material during the crystal growth process. [9] In order for the detectors to achieve high resistivity, some materials like Ge, can be highly depleted of electrically active dopants and reach the resistivity as high as $10^{10}\,\Omega.cm^{-2}$ [50], but for most materials it is unrealistic. Other materials use other methods such as introducing dopants or defects during the crystal growth process to the melting components of the crystal to compensate their existing impurities. [50-51] These dopants and defects can be added during the crystal growth process.

To reach high resistivity by adding dopants to the material, one should be able to balance between donors and acceptors delicately to maintain the Fermi level close to the mid band gap area and achieve a high resistivity. [9] In most materials including CZT, it is very difficult to achieve a precise balance between shallow (low energy level) acceptors and donors. Instead, deep or high energy level defects for compensation are used. [44-45, 51-52] The energy level of these defects is between the Fermi level and valance band of the material and are close enough to the Fermi level that with a small variation in the energy of the Fermi level, a great number of deep levels get ionized and can neutralize the excess

free carriers of the shallow levels. [9] This way the Fermi level never changes dramatically and that is why this technique is called “Fermi level pinning”. [9] At the same time, these deep levels act as carrier trapping centers which contribute to incomplete charge collection and lowering the energy resolution and efficiency. [50-52] Currently most of the CZT crystals grown for radiation detection are grown in Te rich conditions [52] and n-type impurities such as Cl, In and Al are introduced to the material during growth for achieving high resistivity. [44-49] In the material used for this study, Indium was used as principal donor to compensate Cd vacancies as the dominant acceptors.

Other important sources of the point defects are Cadmium or Tellurium vacancies in the material. [9] Based on the Cd pressure during the crystal growth process we can have either singly ionized native donors (Te vacancy) and electrons as the main charged species at high Cd pressures, an intrinsic range with electron and holes as the major charged species in medium Cd pressures or singly ionized native acceptors (Cd vacancy) in low Cd pressure. [53] In Tables 2 and 3 some of the common point defects are presented along with their type (acceptor or donor) and energy levels, respectively. [9]

The detailed mechanism and impacts of defects interacting with carriers is described in the polarization section.

Table 2 - Common traps from groups I, III, IV, V and V with their energy level. [9]

Element	Photoionization, E (meV)	Thermal ionization, E (meV)	Method
Li	Acceptor: 58.0		PL
Na	Acceptor: 58.7		PL
N	Acceptor: 56.0		PL
P	Acceptor: 68.2		PL
As	Acceptor: 92.0		PL
Cl	Donor: 14		
Cl	Donor: 14.48		PL
Cl–V_{Cd}	Acceptor: 120		PL, ODMR
Cl DX1		Donor: 220	Theory
Cl DX2		Donor: 470	Theory
Cl DX3		Donor: 210	Theory
Al	Donor: 14.05		PL
F	Donor: 13.71		PL
Ga	Donor: 13.83		PL
In	Donor: 14.08		PL
In DX		Donor: 300	Theory for $Cd_{0.8}Zn_{0.2}Te$
Ge	Donor: 950	Acceptor: 730	Photo-EPR
Sn	Donor: 850		Photo-EPR
Sn	Donor: 900		DLTS
Sn	Donor: 890, 430		QTS
Pb	Donor: 1280		Photo-EPR

Table 3 - Common traps introduced during growth and their energy levels. [9]

Defect	Thermal ionization, E (eV)	Photoionization, E (eV)	Method
V_{Cd}	Acceptor: <0.47		Photo-EPR
V_{Cd}		Acceptor: 0.78	PICTS
V_{Cd}	Acceptor: 0.2, 0.8		Theory
V_{Cd}	Acceptor: 0.1, 0.4, 0.76		DLTS, PICT
V_{Cd}	Acceptor: 0.1		Theory
V_{Cd}	Acceptor: 0.43		TEES
V_{Cd}	Acceptor: 0.21; Donor: 0.73		TEES
Te_{Cd}	Donor: 0, 0.4		Theory
Te_I	Donor		Theory
Te_{Cd}–V_{Cd}	Neutral		Theory
V_{Te}		Donor: 1.4	Photo-EPR
V_{Te}	Donor: 1.1		DLTS, PICT
V_{Te}	Donor: 0.4, 0.5		Theory
Cd_I	Donor: 0.64		DLTS, PICT
Cd_I	Donor: 0.54		PICT
Cd_I	Donor: 0.5		Theory
Cd_I	Donor: 0, 0.2		Theory

2.5 Extended defects

Extended defects are imperfect structures in crystal, such as dislocations or tilting between two differently oriented crystals. [4] They can also be the assembly of one type of atoms in large amounts. [4] Due to the size of the extended defects being orders of

magnitude greater than point defects (between tens of nanometers to milimeters depending on type of defect in comparison to the point defects with size in range of hundreds of picometers), extended defects are detectable with optical microscopes and chemical methods. [14] Similar to point defects, these defects are causing one of the major drawbacks in CZT radiation detectors that reduce the availability and cost of especially large detectors and are present in even highest quality materials. [14] They cause disturbance in charge collection and limit the production of detectors to small thicknesses and areas. [5] There are several common types of extended defects in commercial detector-grade CZT material that consists of twins, sub-grain boundaries, Te inclusions and dislocations. [9] A brief explanation of each of these defects and their origin comes in the following:

- **Twin and sub-grain boundaries:** These boundaries between different orientations of crystals affect the transport characteristics of charge carriers in severe and different ways. [54] Dangling bonds at these boundaries form a charge barrier for drifting carriers. [54] The electrical conduction along these boundaries also affects the electrical field properties and drift lengths of the carriers. [9] One of the methods used to identify twin and sub-grain boundaries is to etch the surface of the crystal roughly and then shine light on it. In this stage light will be scattered from the surface with different directions due to different crystallographic orientations of the defects and material and the boundaries will be distinguishable with bare eyes [9, 55] While with finely polished samples with electrical contacts it is practically almost impossible to track the boundaries with bare eyes. [14] In these cases that destructive methods like etching is not desirable, methods such as X-ray topography is a suitable choice. [14, 55-56]

- **Mosaics:** Mosaics are in fact slightly tilted sub-grain boundaries. [57] It is believed that dislocations inside the sub-grains are elementary sources of rotation of crystal lattice, resulting in mosaic structures. [57]
- **Te inclusions:** Te inclusions are an important type of extended defects that are responsible for charge distribution distortion in thick detectors. This type of defects have a much smaller bandgap (0.33eV) resulting in highly conductive crystal compared to bulk CZT crystal surrounding it. [9] Typical Te inclusions that are formed during the crystal growth are about 1-30 μm in diameter. [14, 58]
- **Star shaped defects:** These defects are formed during the post-growth annealing process with Cd vapour. It is believed that they are a product of the in-diffused Cd atoms and the molten Te inclusions [59] and appear as star-shaped, highly conductive defects within the crystal. [9]
- **Dislocations:** Dislocations in the CZT crystals are formed during the thermoplastic relaxation in the solid-melt interface during the growth. [56] In high concentrations, these dislocations form dislocation walls that despite having different sources, but act similarly to twin and sub-grain boundaries. They also cause severe non-uniformity in the charge transport, which indicates distortion of the electric field inside the detector. [55-56, 60-61] Methods of detecting them are also similar to those of twins and sub-grain boundaries (Rough etching/polishing). [14, 55-56, 62]

2.6 Polarization

As briefly mentioned in the previous chapters, polarization is a result of point defects introduced to the material during growth [5] and are one of the most challenging barriers

in obtaining high yields in fabrication of CZT radiation detectors. [63-65] This causes the output count-rate and peak position of detectors to move noticeably. [63-66]

Free carriers travelling in the electric field induced by the bias voltage across the detectors can be trapped in the point defects present in the crystal. This results in the build-up of charge carriers and non-uniform distribution of electric field over the detector shown in Figure 8. [5] This affects the drift velocity of the carriers, which is eventually decreased and causes even more carriers to be trapped. [5]

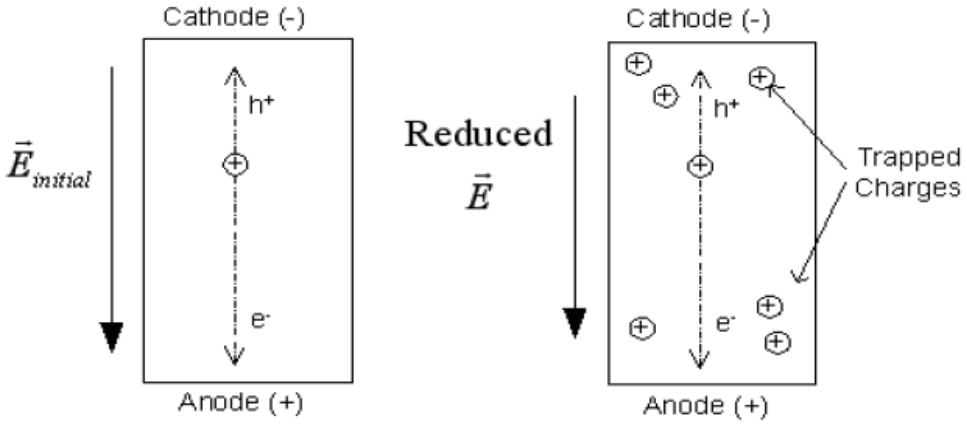

Figure 8 - Polarization in radiation detectors. By producing more carriers they have been trapped in the trapping centers present in the material. This charge accumulation has resulted in reduced electric field. [5]

There is a de-trapping time (τ_e and τ_h for electrons and holes respectively) [67-68] associated with the time a charge spends in a trap, which is mainly controlled by temperature and energy of the trap. [42] The lower the temperature, the less energy carriers have to spent to overcome the energy barrier of the traps to set themselves free. In the extreme case, the lifetime of the carriers is much smaller than their de-trapping time and they are called “frozen”. [69]

There are two types of traps resulting in polarization of detectors. One is the hole trap, trapping slower travelling holes and causing build-up of positively charged carriers and affecting the electric field, [63-66] the other type is the electron trap, mainly in deep energy levels that are inactive in the normal conditions. [70-71] First type is believed to be responsible for polarization of detectors when X-ray is illuminated [28, 66] and the second type is responsible for bias induced polarization and instability of the detectors. [70-71] Both types of polarization mechanisms will be discussed in more details in the following chapters.

2.6.1 X-ray induced polarization

One of the most frequently observed cases in which polarization affects the performance of the detectors is when they are under X-ray illumination. [5] It causes a great number of excess carriers to be generated [63] and start travelling towards anode (for electrons) and cathode (for holes). Hole trapping centers mostly caused by impurities introduced to material during growth process are believed to have energies greater than Fermi level and close to the conduction band, which are usually referred to as shallow energy traps, and thus are empty and active in the bulk of the material in the equilibrium condition and slow-moving holes get trapped in those centers. [63-65] This causes the disturbance of the electric field in a way that most of the electric field and voltage drop will occur in the region closer to cathode, where carriers were generated in the first place and only a small portion of the electric field will remain for the rest part of the detector. [5, 63-66] This results in a lower drift velocity of the electrons in the area [5] with low electric field and as a result more holes will get trapped and the performance of the detector degrade dramatically. [64] This phenomenon is illustrated in Figure 9. In part four, a comparison

between electric field distribution under dark condition and under X-ray illumination is shown. In the latter case most of the field drops within the first small portion of the detector depth.

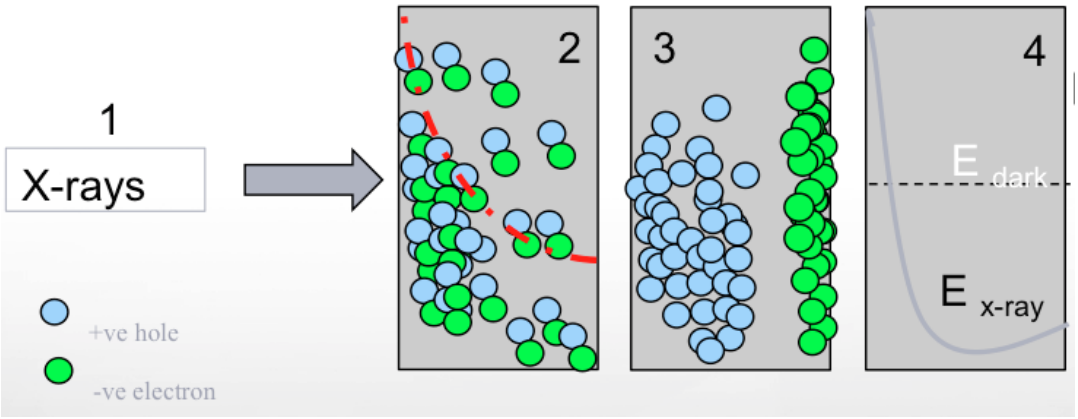

Figure 9 - Polarization of carriers induced by X-ray illumination. Faster electrons are collected by anode where holes are trapped in the trapping centers and caused distortion of electric field. In part 4 you see the effect of this trapping on the distribution of the electric field under X-ray illumination.

2.6.2 Bias induced polarization

Another case in which polarization may occur, even before illumination of X-ray is when the bias over anode and cathode is applied in order for the electric field in the detector to be generated. [70] In this case the electron traps which are normally filled in the bulk of the material come to play. In the bulk of the material, Fermi level is well above these traps [70] and they are occupied by an electron and are neutral but if the Fermi level moves below the trap level, it will be empty and positively charged. [70] As discussed before Fermi level in CZT material used for detector fabrication is usually pinned to near mid-gap energy in order to increase the resistivity of the bulk material. [9] The materials used for this study are slightly n-type, so the Fermi level is slightly higher than the mid-gap energy band. Figure 10 shows a schematic of a donor trap in both de-active and active modes. [70]

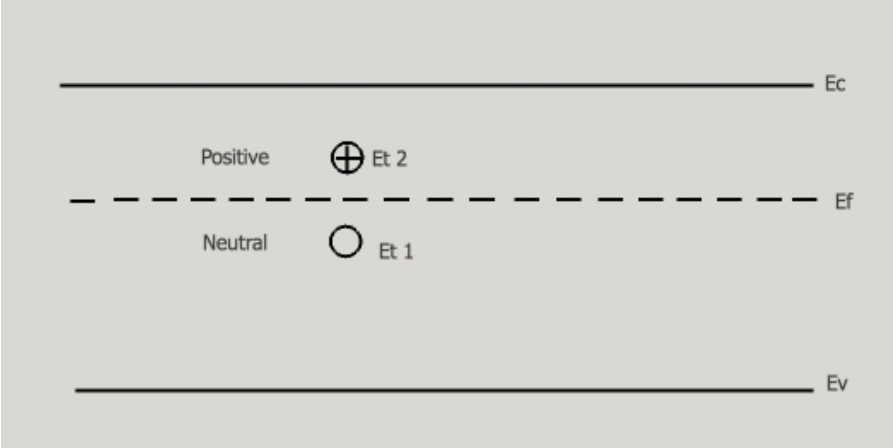

Figure 10 - Energy level of donor traps in both filled and empty cases. It has neutral charge in the empty case and it is active and positively charged when empty.

The behaviour of the energy bands near the metal-semiconductor contacts of the anode and cathode after applying bias voltage can be of interest in terms of traps occupancy. Based on Schottky-Math theory, metals with high work functions like Gold or Platinum (with work functions 5.1eV and 6.35eV, respectively) tend to have blocking contacts with n-type material and ohmic with p-type. [71] In semi-insulating materials like CZT, high work function metals form blocking contacts with electrons and ohmic with holes. [71]

In the detectors used for this study, Platinum is used as the anode and cathode metal. When negative voltage is applied in cathode and positive voltage to anode, presented in Figure 11, the energy bands bend due to the Schottky contact generated at the metal-semiconductor interface. [70] As the position of the Fermi level in a certain material is constant, band bending causes the deep energy level traps to go above the Fermi level on the cathode side. These traps are then empty and active and can contribute to trapping of electron carriers. [70-71] If the number of these traps is high enough, they cause noticeable

trapping even before the X-ray illumination. Equation 2.7 shows the relationship between ionized deep donor traps and time after applying bias voltage.

$$\Delta N^{+}(t) = N_T[1 - \exp(-\frac{t}{\tau_c})] \quad (2.7)$$

Where N^+ is the concentration of ionized traps, N_T is the number of traps at t=0 and τ_c is the de-trapping time given by:

$$\tau_c = \frac{1}{N_C \sigma \nu} \exp(\frac{E_T}{KT}) \quad (2.8)$$

Where N_c is the effective density of states at the conduction band, ν is the thermal velocity of the electrons, E_T is the trap ionization energy relatively to the bottom of the conduction band and σ is the electronic capture cross section.

As you can see number of activated traps increases with time, which causes instability of detectors over the time.

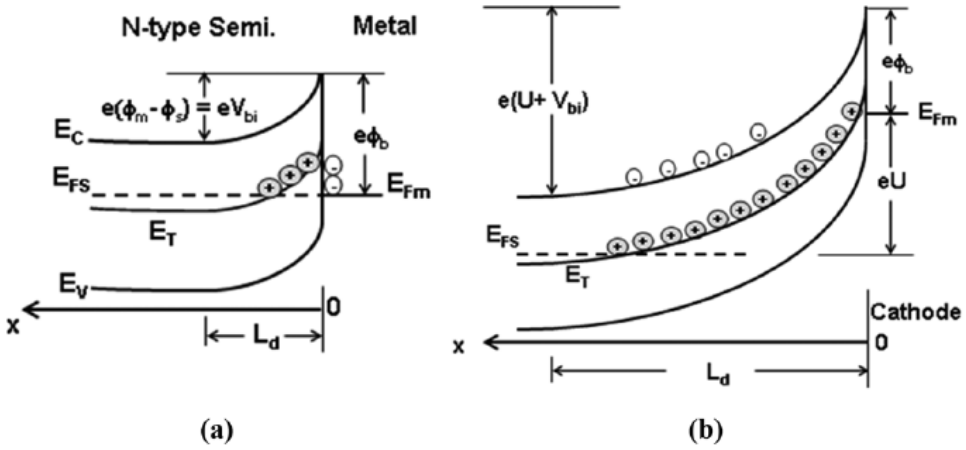

Figure 11 – Energy band diagram showing the band bending close to the metal-semiconductor surface, a) under no bias and b) under reverse bias. φ_m, φ_s, E_{fm} and E_{fs} represent the work functions and Fermi levels of the metal and semiconductor, V_{bi} is the built-in potential of the barrier and L_d is the depletion region's width. Under the reverse bias more of the donor traps have an energy level higher of the Fermi level and get activated. [70]

2.7 Charge steering and charge channelling

Charge steering and charge channelling are other examples of detector performance degradation due to extended and point defects present in the CZT crystal. These phenomena cause distortion in the carrier collection mechanism and signal formation of the detectors.

- **Charge steering:** Charge steering or lateral polarization refers to the lateral movement of the carriers with respect to the electric field in the detector, instead of the expected direction from the cathode to the anode. This is caused by extended defects affecting the transfer of carriers along the detector. [72] Typically, there exist two types of charge steering, dynamic and static. [4, 72]

  Dynamic charge steering is caused by the slower hole carriers. [72] Due to their slower speed, they could be trapped in the hole traps present in the material and create accumulated charge. The traps can act as a barrier for the carriers to pass and result in a dark, lower output count area in the output. [14, 72]

  Static charge steering is related to charged structural defects [72] that guide the carriers away from them and result in a low output count area corresponding to the shape of the defect. [14, 72]

- **Charge channelling:** Charge channelling occurs when extended defects such as twin boundaries are present. [73] These boundaries are usually decorated with Te inclusions, which are highly conductive. [30] Consequently lots of the carriers will be attracted towards these boundaries and will form lines with high output count-rates called “hot lines” in lower output count-rate or “cold” surrounding. [30]

3 Materials and methods

In this chapter methods and materials used to study the CZT material and radiation detectors are introduced. These methods can be divided into four main categories: optical techniques, electrical methods, chemical methods and operational methods. Each category will be described in more details in the following sections.

3.1 Optical techniques

Optical techniques use light as to study the characteristics of the CZT crystal. In this project IR imaging was used as a tool to inspect the CZT crystal quality and extended defects present in it. Pockels effect was used to measure the electric field distribution inside the detectors, which can give us valuable information on defects and charge distribution. Deep level transient spectroscopy was also used as a method combining optical and electrical means to study the presence of point defects specifically. The working principals of each of these methods are explained in the following sections:

3.1.1 IR imaging

Infrared (IR) transmission microscopy and its deviations (such as Fourier transform infrared microscopy) are well known methods of material characterization. [9, 74] CZT crystal is opaque to visible light but transparent to IR light. Extended defects however, have different optical properties and are opaque to IR light. Consequently, they form dark spots in the IR image. [14]

As illustrated in Figure 12, the IR imaging system used in this study consists of an IR source illuminating from the bottom of the sample, some mirrors to focus the light on the sample, the aperture to condense the light and IR detector to sense the output.

Figure 12 – a) A simple schematic of IR microscopy. IR light is illuminated on the sample from the bottom and is detected by the IR detector on top of the system. b) IR Microscopy used in this study at Redlen Technologies.

This method of spectroscopy is useful in recognizing extended defects such as Te inclusions and twin or sub-grain boundaries, but cannot help in studying the point defects inside the crystal.

3.1.2 Pockels electric field measurement

In materials with Zinc-blende structure, the refractive index can be modified anisotropically so that the crystal becomes birefringent under applied bias voltages. This effect is called the Pockels effect. [14] Birefringence is defined as the double refraction of light in a transparent, molecularly ordered material, which is explained by the existence of orientation-dependent differences in refractive index. [62, 75]

After applying the Pockels effect in the material, the electromagnetic vector of the light rotates with the intensity of the electric field inside the detector. [14] Then by inspecting

the light intensity inside the material, one can measure the electric field distribution. Quantitatively, the light intensity inside the material follows: [14]

$$I = I_0 \cdot Sin(\partial) \tag{3.1}$$

Where I_0 is the maximum transmitted light through the detector, I is the difference between light intensities with and without the presence of bias voltage. ∂ is the holdup angle of the light inside the crystal, expressed as: [14]

$$\partial = \frac{\pi \cdot {n_0}^3 \cdot r \cdot d}{\lambda} \cdot E \tag{3.2}$$

Where n_0 is the field-free refractive index, r is the linear electro-optic coefficient, d is the path length of light which in our case is the thickness of the crystal, λ is the light wavelength and E is the electric field intensity.

By having the electric field distribution inside the detectors we can gain valuable information about the effect of crystal defects on the performance of the detectors. In Figure 13, the Pockels set-up used for this study, belonging to Redlen Technologies, is presented.

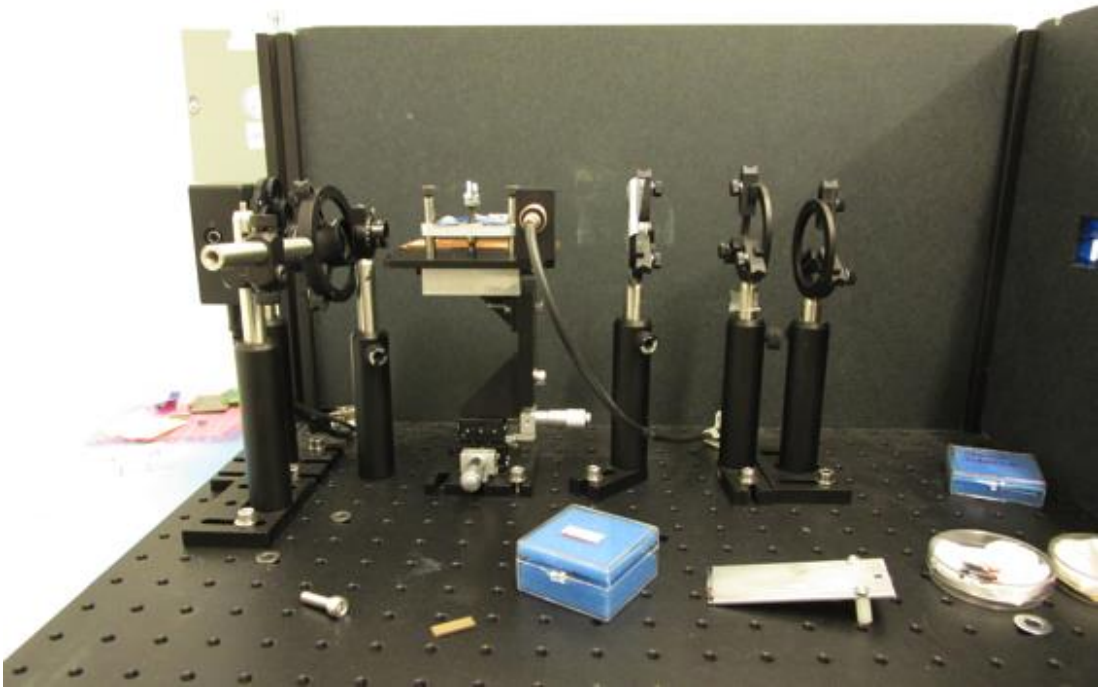

Figure 13 - Pockels system set-up used in this study, belonging to Redlen Technologies. Light is illuminated by a source on the right side of the box and after passing through two polarizers enters the sample. The light detector is placed on the left hand-side of the box and the output signals goes to the computer and translated into electric field using the aforementioned relationships.

3.1.3 Deep level transient spectroscopy (DLTS)

The basic working principle of DLTS is shown in Figure 14. It works by changing bias voltage of a p-n or Schottky junction, which in our case is the metal-semiconductor junction between the cathode and the slightly n-type CZT crystal, in different temperatures and measuring the time constant the system needs to reach the steady state condition. [76-77] Because of the gradient in charge carriers' distribution, majority carriers of each material diffuse to the other side of the junction, leaving oppositely charged ions behind. These ions form an electric field opposing the direction of diffusion current, so at a point the drift current caused by this electric field opposes the diffusion current and the material reaches

equilibrium. [4] (Seen in part a of Figure 14). The area that is almost empty of free carriers is called depletion region and it mostly penetrates through the material with lower concentration of dopants. (For the metal-semiconductor junction it only penetrates into the semiconductor as metal has much greater number of free carriers in comparison to semiconductor) [4, 14]

In the DLTS method, in each temperature step, a pulse of bias voltage (in this case forward bias) is applied on the junction, which causes the depletion region to narrow down because of the opposing external electric field and the majority carriers to go back and fill some of the depleted area of their side of the junction and so the traps in the depletion region that were empty of free carriers also get filled [78] (part b of Figure 14). After the pulse period is finished, depletion area width tends to go back to what it used to be, [76] so the carriers have to immigrate back. This process happens much fast for the conduction band electrons rather than the trapped carriers as they have to overcome the trap energy barrier first.[76, 78] The higher the temperature is the easier it gets for carriers to overcome the low energy traps, so in higher temperatures we can sense traps with deeper energy levels. By measuring the capacitance of the junction we can monitor the time corresponding to the system to reach the steady state in each temperature. [74, 78] This transient time is an exponential function with the constant equal to the thermal emission rate of the traps. [79] Also, the peak of the capacitor amplitude after the pulse is removed is proportional to the density of traps present in the material. [79] Therefore, this method can give us valuable information about the traps present in the material.

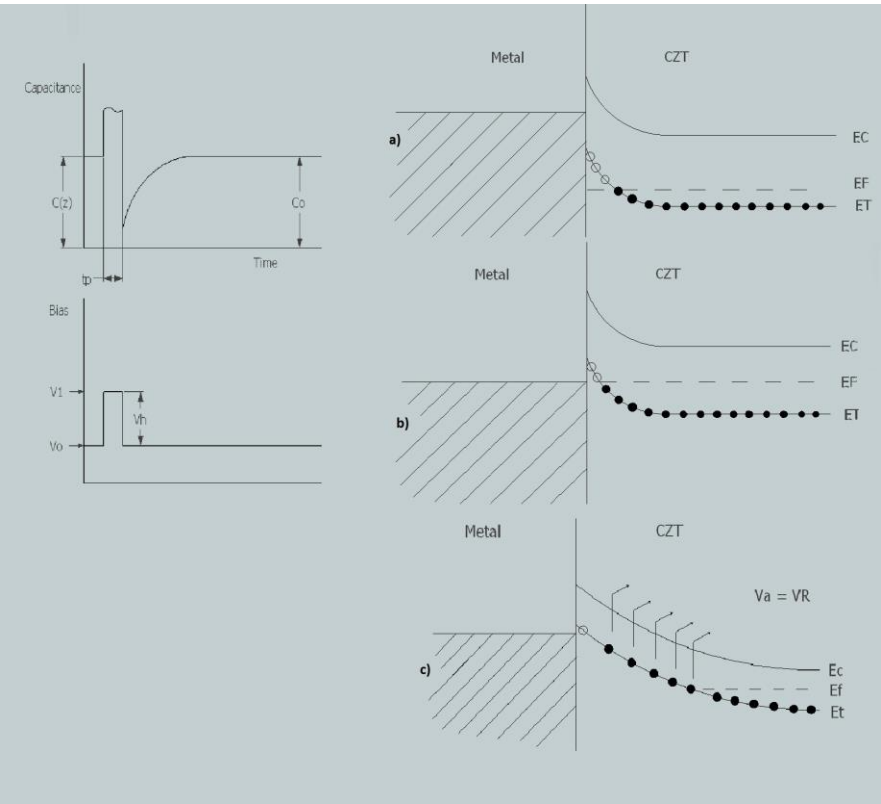

Figure 14 - On the left hand-side the sudden pulse and change in the junction capacitor is shown. On the right hand-side the traps occupancy before, during and after the pulse is shown. By measuring the time constant of the junction capacitor change and repeating this measurement in different temperatures we can find the density, cross section and energy level of the traps. [77]

3.2 Electrical techniques

These methods rely on the electrical properties of the CZT material to monitor their resistivity or capacitance. DLTS was earlier discussed in the optical techniques section as a method using both optical and electrical properties of the material to identify the point defects. Here the contactless resistivity mapping method and how it can help us recognize either extended or point defects are explained.

3.2.1 Contactless Resistivity Mapping (CoReMa)

This method can give us a full map of material resistivity in wafer or detector size level without having an ohmic contact with the material. [80] It is a rapid, non-destructive tool that has a resistivity detection range of $1 \cdot 10^5$ to $1 \cdot 10^{12}$ ohm-cm. [80] The probe size and therefore each scanning step can vary between 100 μm to 1 mm in diameter which can be adjusted based on the desired resolution. [77, 80]

The principle of this technique is based on the self-discharge of the free carriers in a semiconductor after applying a charge pulse. [80] The schematic of the CoReMa system as well as its hardware representation is illustrated in Figure 15.

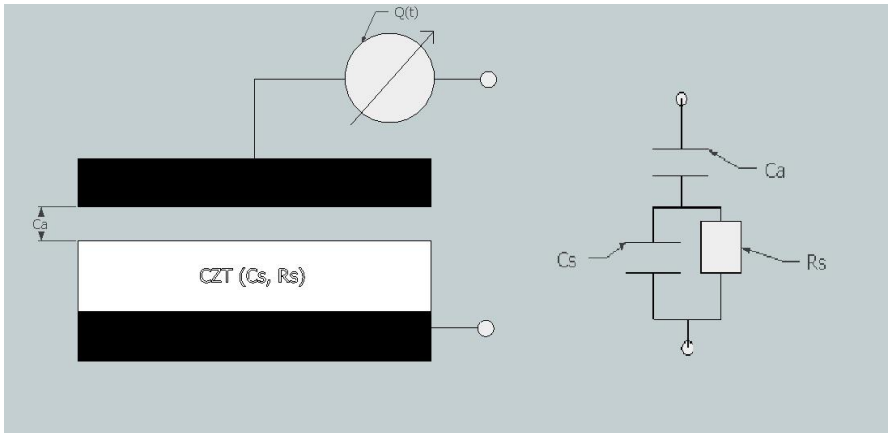

Figure 15 - a) Schematic of the CoReMa system, b) Equivalent circuit of the system. By applying voltage over the system and measuring the current we can find the equivalent resistivity and capacitance of the CZT crystal. [80]

There is the C_S and R_S representing the equivalent resistance and capacitance of the semiconductor and C_a stands for the air gap capacitance. When the charge pulse is applied to the system both C_a and C_S capacitors are charged. Without removing the charge pulse C_a will remain charged but charge stored in C_S will start being discharged in its parallel resistor, R_S. So we can say the charge in the moment t=0 equals to:

$$Q(t=0) = \left(\frac{C_s \cdot C_a}{C_s + C_a}\right) \cdot V \quad (3.3)$$

Where V is the applied voltage and the charge after C_S is discharged equals:

$$Q(t=\infty) = C_a \cdot V \quad (3.4)$$

So by comparing the charge in the beginning and after it reached its stable value, we can calculate C_S. [80] The time constant of the charge decay can also give us the value of the parallel resistor R_S in which C_S was discharged. By repeating this process over the whole wafer we can have a resistivity map of the wafer, which can be very helpful in inspection of defects in crystal due to different resistivity of the bulk of CZT and different types of defects. [77, 80] A sample of the charge-time variations is shown in Figure 16.

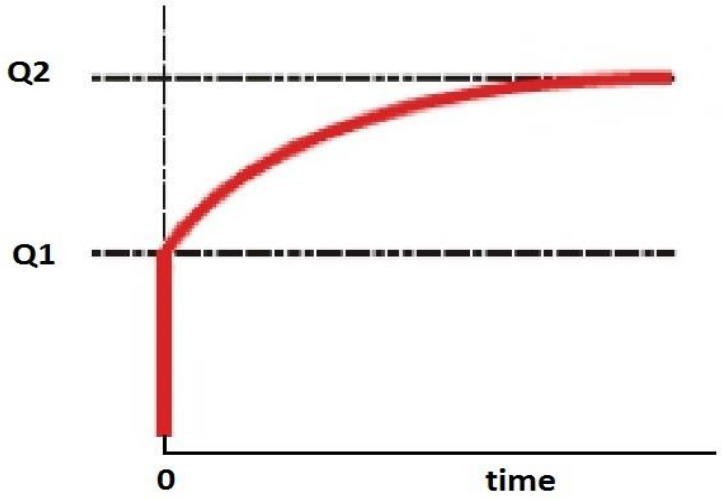

Figure 16 - An example of charge-time output signal of the CoReMa system.

3.3 Chemical methods

These methods use chemical solutions to distinguish between different crystalline structures in the CZT material. Etch pit density mapping was used in this study to study the extended defects present inside the CZT crystals.

3.3.1 Etch Pit Density (EPD) mapping

EPD mapping is a commonly used method for extended defect recognition. [9, 14, 81] In this method, the CZT substrate is treated with Nakagawa etchant solution ($HF:H_2O_2:H_2O$ 3:2:2). [81] Due to different crystal orientations and different structural properties, the etch rate of the defects and the bulk CZT are different, [81] so after the etching process one can count the etch pits caused by impurities in the crystal in some random sub-fields from different parts of the wafer under microscope. This number can be an indicator of crystal quality. The shortcoming of this method is that it is a destructive method for the surface of the crystal and the chemicals used in the process are extremely dangerous. [9]

3.4 Operational measurements

This type of measurement, which we called it operational measurement, evaluates the performance of the detectors, real time, under application-specific working conditions using the in-house high flux tester instrument in Redlen Technologies.

3.4.1 High flux tester

High flux tester is a commercial tool that is the proof of concept for medical applications that require high input fluxes of X-ray. This method of characterization can give us a very good picture of both extended and point defects within the CZT detector and their role. In this method an X-ray beam is used to monitor the performance of the detectors. This beam is generated in an X-ray tube, where electrons are accelerated under very high voltages and hit a Tungsten metal target, creating accelerated, high-energy photons. [74] In Figure 17 the X-ray spectra of energy before and after filtration with 1mm Cu and 1.5m Al is presented.

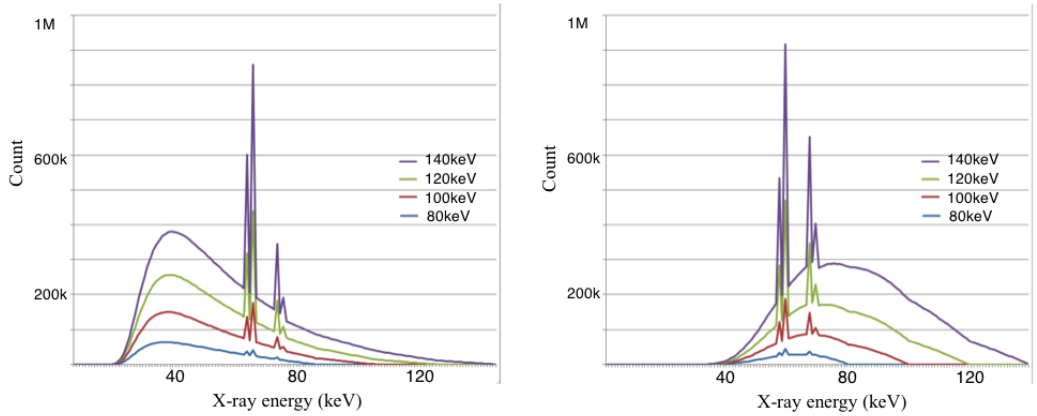

Figure 17 - X-ray spectrum of energy before and after filtration with 1mm Cu and 1.5mm Al. The output peak has shifted from lower energies to higher energies, which make it more distinguishable from noise.

In Figure 18 a picture of the in-house X-ray machine at Redlen Technologies, used in this study, is shown. The sample is placed at the bottom of the machine and the X-ray is illuminated on the cathode side of the detectors from the top after passing through 1mm Cu and 1.5mm Al filters. Sample is mounted on top of the application-specific integration circuit (ASIC) and the proper connections to anode and cathode are made through the rubber balls on the ASIC that can be precisely aligned with the anode pixels and conductive rubber between cathode and the metal to ensure proper electrical connection between the high-voltage supply and the cathode, respectively.

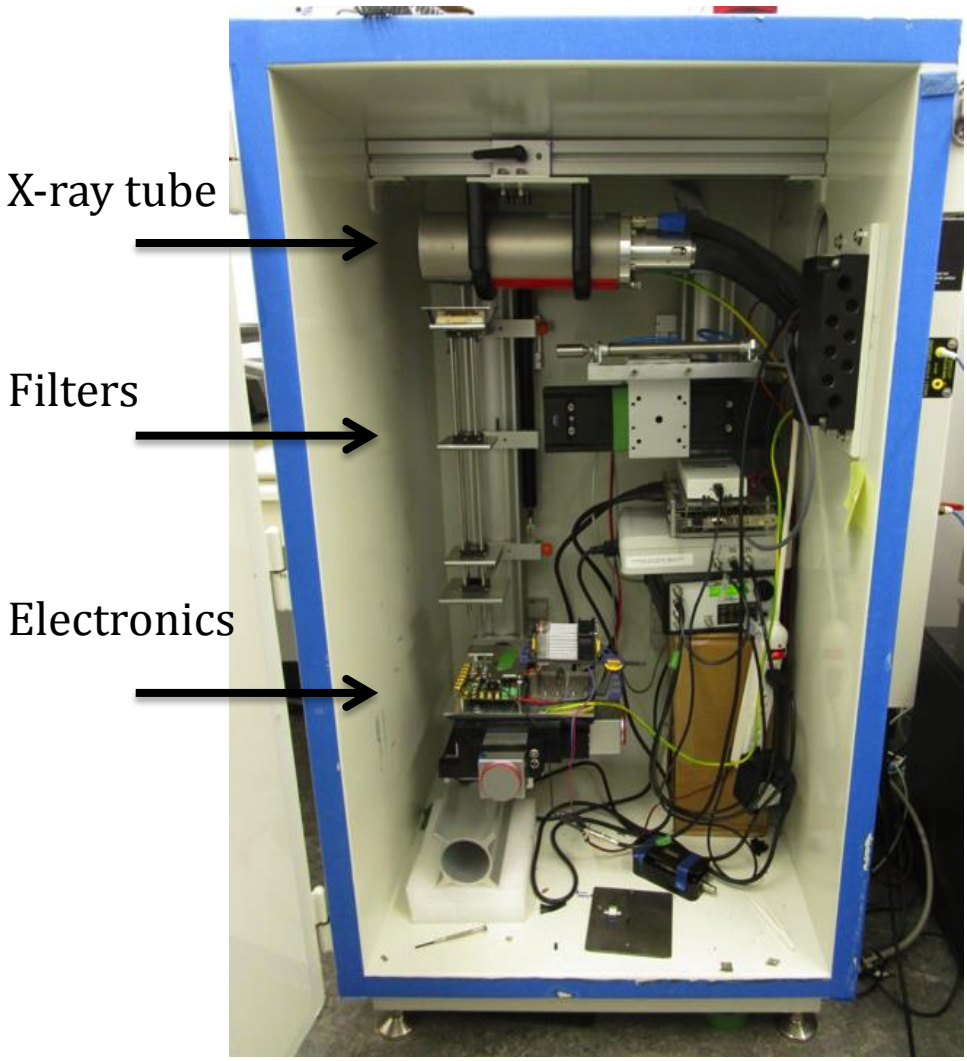

Figure 18 - In-house X-ray test system provided by Redlen Technologies for this study. The X-ray illuminates on the sample from the top and signal is read by ASIC circuit on the anode of the detector.

One of the important outcomes of this measurement is Output Count-rate (OCR) map. In this map the number of detected photons in each pixel is counted and can be translated into colors for each of the corresponding pixels. The result is a full pixelated map of the detector, showing its overall performance in terms of photon sensing. Another important data that can be extracted from this test is the linearity of output count-rate versus input count-rate, which indicates the ability of the detector to work under high input X-ray fluxes.

Extended defects are easily traceable using the OCR map of the high flux tester. They either cause charge steering which appears as darker areas (cold areas) with lower number of output counts or charge channelling that creates high number of output counts also known as hot areas. Point defects on the other hand, do not appear directly in the OCR map but by comparing the results of the detector's behaviour with different applied biases and without or with X-ray illumination or even in different temperatures, one can obtain information about the effect of point defects in the material.

Because of the advantages mentioned above in tracing both extended and point defects inside the CZT crystals and the ability to examine the performance of the detectors under different operational conditions, this method is the main method of interest for characterization of the CZT detectors in this study.

4 Results and Discussion

In this chapter the results of the experiments and measurements on samples with different qualities using different measurement systems, followed by discussions on those results and relationship between them are presented. They are divided in two parts, X-ray maps with extended defects, and with point defects. As discussed earlier, extended defects are visible so it is easier to track them and specify their types, point defects on the other hand cannot be seen visually, but there are methods that they can be sensed through them.

4.1 X-ray maps with extended defects

In this section a number of detectors with extended defects were recognized by the X-ray tester. These detectors were later studied using other characterization methods in order to find a meaningful relationship between the results. The effects of operational condition on the extended defects in the crystal and in general on the performance of the detectors were also examined.

4.1.1 X-ray tester versus EPD mapping

Using the X-ray measurement system introduced before we can obtain the output count-rate maps of samples under different intensities of X-ray illumination, with different biases on the samples and even in different temperatures. In Figure 19 the output count-rate map of sample number one under high input X-ray flux is shown. All the samples used in this study are fabricated using Redlen's standard radiation detection fabrication process and have a pixelated area of 22×32 pixels of $500\mu m \times 500\mu m$ resolution. The counting maps are measured with the X-ray high flux tester shown in Figure 18 and the circuit used for read-out of the signal is the ASIC with photon counting mode described earlier. In this

measurement the X-ray tube current was 25 mA and a bias of 700V was applied over the sample. Dark regions represent poor charge collection and limited signal.

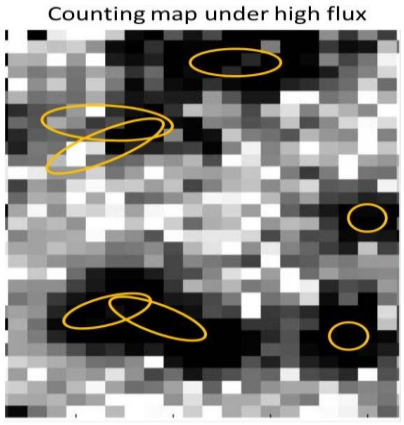

Figure 19 - Output Count-rate map of sample number one under high flux of X-ray. Darker regions marked by yellow circles represent lower output counts.

Non-uniformity in the output count-rate map of sample number one motivated us to test it with EPD method too. As the EPD mapping requires working with dangerous chemicals, this part was done by trained technicians in Redlen Technologies under supervisory of my colleague Pramodha Marthandam. The results of this EPD mapping are presented in Figure 20.

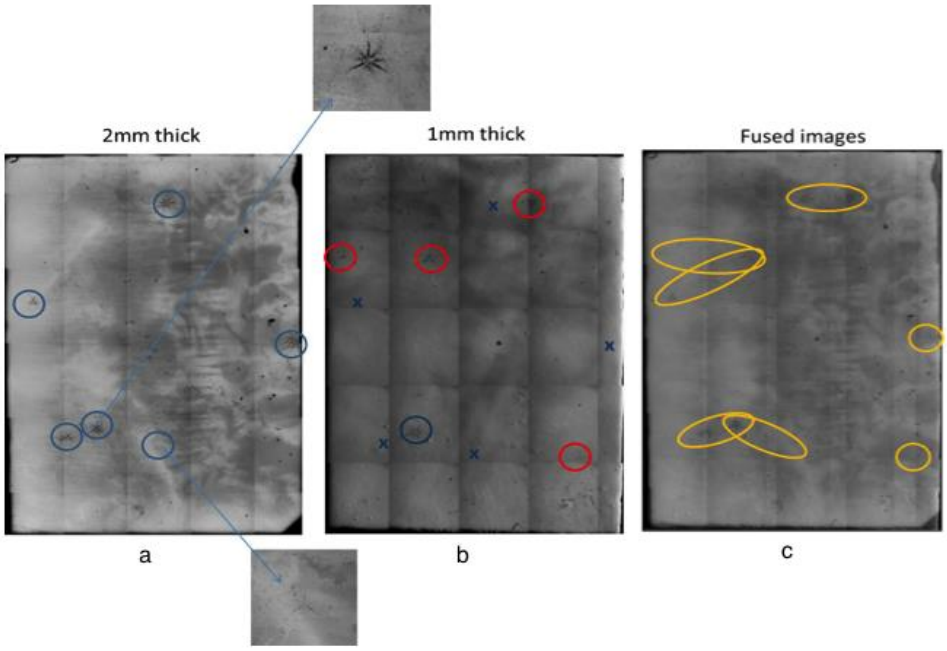

Figure 20 - EPD maps of a) detector number one on the surface, b) after polishing of 1mm and threating with EPD again and c) the fused image. The resulted patterns of the fused image show high compatibility with the result of high flux tester.

First picture on the left shows the EPD map of the surface of the detector. Several star-shaped defects can be seen on the surface of the material and have been marked with blue circles. To investigate if these defects are extended in depth of the detectors too, 1mm of the detector thickness was polished off and the sample went through the EPD mapping process again. The result is shown in the middle picture of Figure 20. As the figures suggest only one of the star-shaped defects present on the surface of the material extended in depth of the material. Red circles present defects that did not exist on the surface of the material. The picture on the right hand-side of Figure 20 is the fused image of the two surface and 1mm depth EPD images of sample number one. The yellow circles, showing the location of star-shaped defects through the detector show very good agreement with the yellow circles representing the lower count-rate areas of the X-ray map in Figure 19.

In another similar test with sample number two, the high flux test and EPD mapping were performed on the sample, under two different bias voltages and the results can be seen in Figures 21 and 22, respectively.

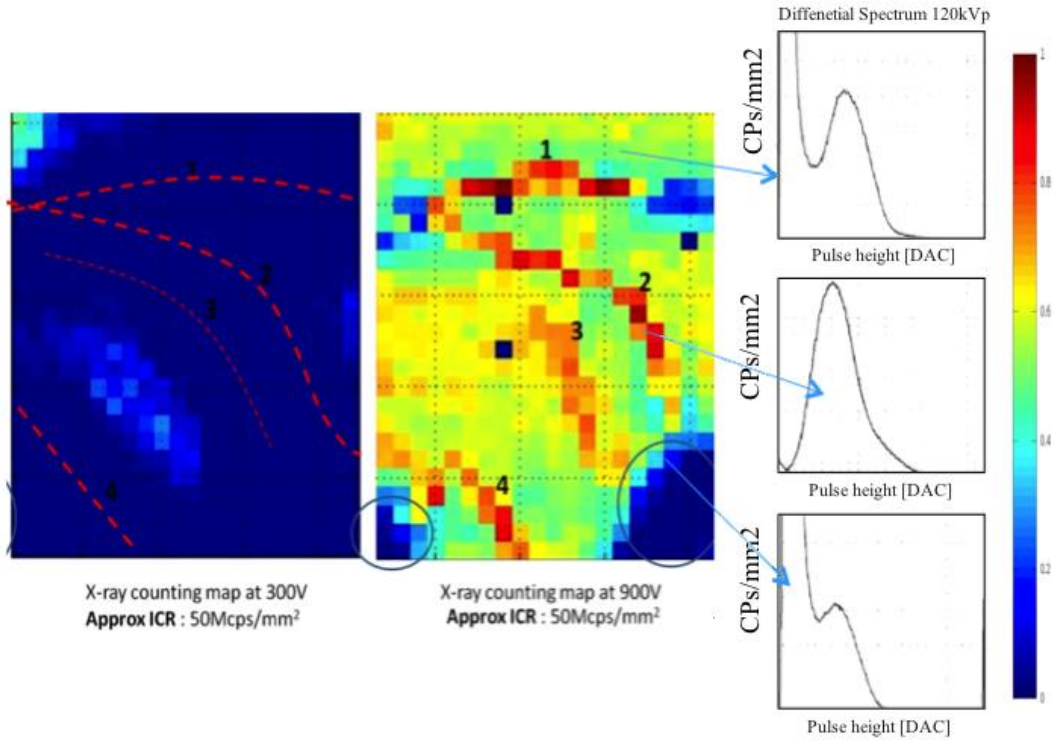

Figure 21 - Output count-rate maps of sample number two under low bias (300V) and high bias voltage (900V) and 120kVp, 1mm Cu and 1.5mm Al filtered differential spectra for three different selected pixels. Red dashed line shows where the hotlines under 900V bias are present. Blue circles represent the low output count-rate areas. The spectra show that for hotlines there is an extreme peak of X-ray whereas for the low output count-rate area shown by bly=ue color, the X-ray peak is very weak and in low energies.

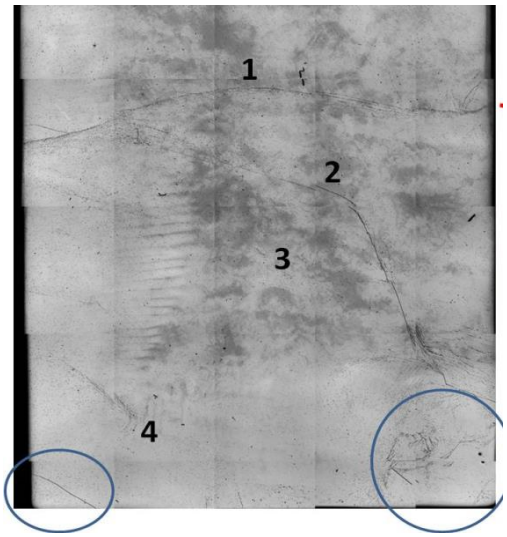

Figure 22 - EPD map of detector number two. sub-grain boundaries and mosaics found with this method match well with the hotlines and low output count-rate areas of the high flux tester result.

In this experiment, there are a number of interesting observations. By investigating to the EPD image of the surface of the detector, we observed that there were two types of extended defects present. One is the sub-grain boundaries, numbered one to four on the detector map, which is usually decorated with low resistivity Te inclusions and the other one is the mosaics marked with blue circles on the corners of the detector.

As the figures suggest the sub-grain boundaries resulted in a high output count-rate in the X-ray map whereas the mosaics resulted in dark, low output count-rate areas.

The X-ray spectrum for three selected pixels, one in low counting are, one in the good area and one on the hot line areas of the detector are also shown in Figure 21. The difference between the spectra in the three areas is noticeable. The spectrum of the pixel in the good area shows a distinguishable peak, where the peak of the spectrum in the low output count-

rate area is shifted and weakened and almost merged with the noise. The hotline area shows an extremely high peak.

It is also interesting to notice how the bias voltage affects the output count-rate map of the detector. As discussed in the theory section, the bias between the cathode and anode forms the electric field, which helps the carriers travel in the detector and also controls their drift velocity. The lower the bias voltage is, fewer carriers can make it to the contacts and we have a weaker output count-rate, where we cannot distinguish between different areas of the detector very clearly.

4.1.2 Effect of input X-ray flux and biasing voltage on the detectors' performance

To clarify the effect of different X-ray input photon fluxes and bias voltages more, we designed an experiment in which in one case the bias was kept constant (900V) and the X-ray tube current (flux) was changing from 1mA to 25mA and in the second scenario the

tube current was constant and set to 25mA and the bias voltage was changing from 100V to 1000V. The results of these tests are shown in Figures 23 and 24 respectively.

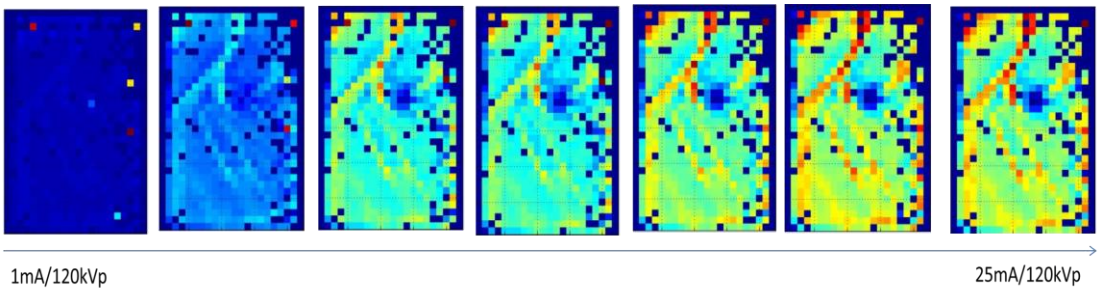

Figure 23 - Evolution of detector number three performance under constant bias (900V) and different X-ray tube currents varying between 1mA to 25mA. Pattern of the dead areas and hotlines have not changed with increasing the input X-ray flux.

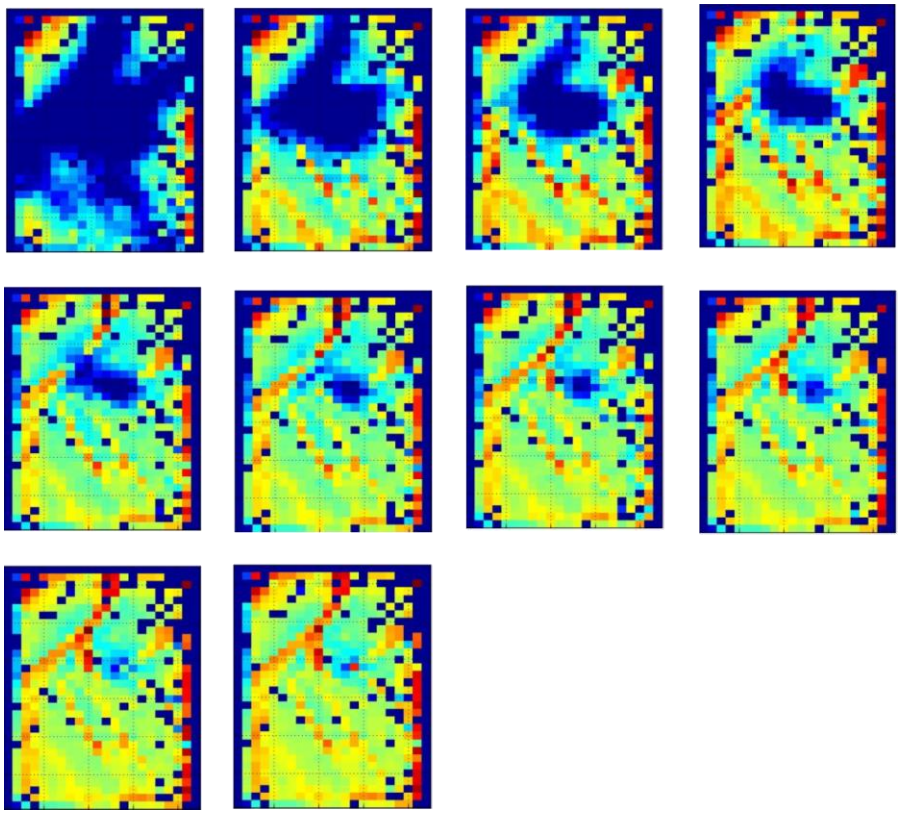

Figure 24 - Performance of detector number three under constant X-ray flux (25mA) and varying bias voltages from 100V to 1000V. By increasing the bias voltage the dead area comes back to life.

Interestingly, in the first test with the constant bias and varying photon flux, you can notice that the regions with extended defects, which are consisted of a circular low-count (cold) area plus numerous hot lines, are distinguishable from the very low fluxes and their shape does not change with increasing the flux. Only the number of the output counts increase, which is simply because of increase in the input photon counts. Conversely, in the second experiment with constant flux and increasing bias voltage, we can clearly see that the shape and size of the cold area is changing and when applying high voltages (around 1000V) this area is completely restored again.

4.1.3 High flux tester versus IR microscopy

During the high flux testing of detector number four, severe hot lines and extended defects were observed. The output count-rate map of this detector is presented in Figure 25.

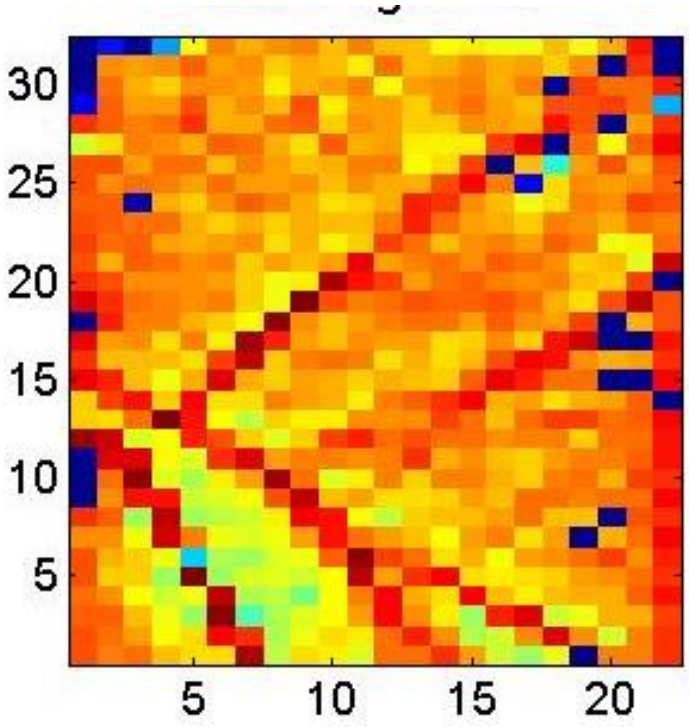

Figure 25 - Output count-rate map of detector number four with 900V bias and 25mA X-ray tube current. Severe extended defects can be observed.

To investigate the source of the problem, the detector was imaged using IR microscopy. As the contacts were already fabricated and we didn't want to remove them, the images were taken from the side of the detector, showing extension of defects through the depth of the detector. In Figure 26, the IR images of areas corresponding to hot lines in the detector are shown.

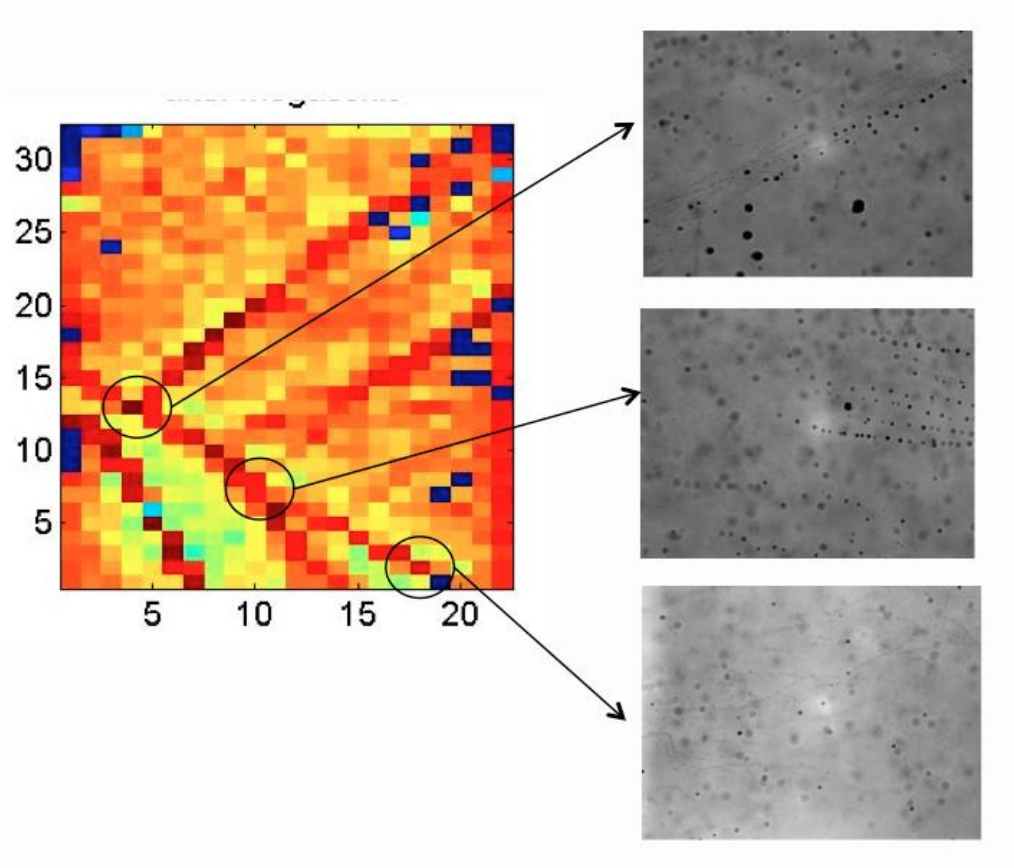

Figure 26 - Output count-rate map of detector number four on the left and IR microscopy images of different spots of it on the right. It should be noted that IR images are taken from the sidewall, so there are along the depth of the detector. Frame size of IR images are 0.89mm × 0.67mm.

The figures confirm that the hotlines in the output count-rate map correspond to twins decorated with Te inclusions in the IR images.

4.1.4 CoReMa mapping versus EPD mapping

By being able to screen the quality of the CZT crystal even before fabrication, in the wafer level, we can reduce the fabrication costs and efforts by eliminating the parts of the material with visible defects that are proved to have degrading effects on the performance of detectors. Contactless resistivity mapping (CoReMa) as introduced before, is one of the methods that can screen the material in the wafer size level without leaving any harm to

the material. EPD mapping can also be used for identifying the extended defects inside the material but has the disadvantage of damaging the surface of the crystal and thus affecting the conductivity of the surface and semiconductor-metal interface quality. Figure 27 shows the wafer level screening of CZT crystal grown by THM method in Redlen Technologies using CoReMa and EPD mapping for wafer number one.

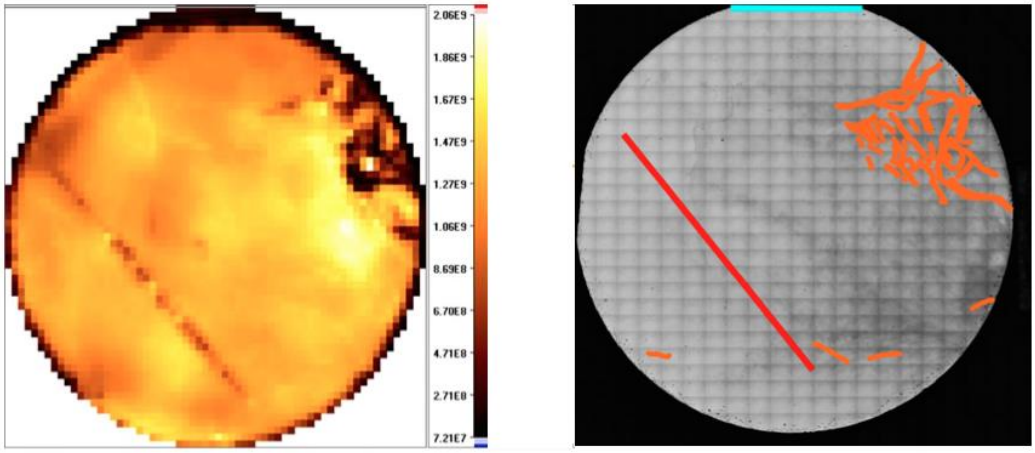

Figure 27 - High resolution CoReMa image (left) and EPD map (right) of CZT wafer one grown by THM method in Redlen Technologies. Twin line running through the wafer is traceable in images taken using both methods.

As the CoReMa map suggests wafer number one has uniform resistivity, but you can clearly see the high conductive line in it, which matches with the twin boundary seen in the EPD map.

4.2 X-ray maps with point defects

This section is dedicated to studying the presence and effects of the point defects in the CZT crystals. Major types of point defects or traps present in the crystal are studied using various characterization methods. Similar to the last section, effects of operational

conditions on these defects and general performance of the detectors were also investigated.

4.2.1 Polarization in different generations of Redlen's detectors

In this section, three different detectors, from three generations of Redlen's detectors, numbered five, six and seven, respectively, were tested using the X-ray high-flux tester. Generation 1 detectors needed high electric fields to operate (600 V/mm) and also high temperature (≥40°C), the second generation still needed the same high electric field and high temperature but could operate to a higher input count-rate point, whereas the third generation works with electric field as low as 150 V/mm and in room temperature. The higher electric field in the earlier generations would help the detectors to have higher carriers drift velocity, which would result in lowering the number of carriers trapped and the higher temperature would allow the carriers to have higher energy to overcome the traps' energy and become free. The output count-rate of these detectors versus their input count-rate is plotted in Figure 28.

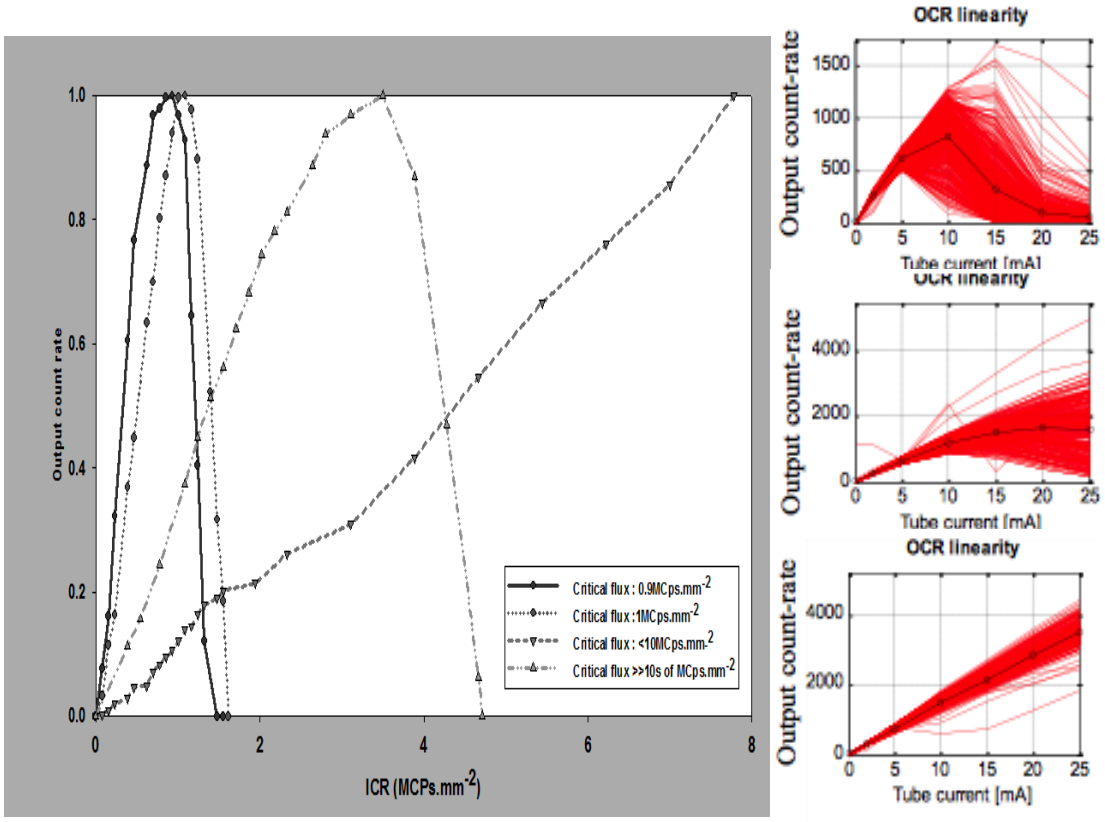

Figure 28 - Output count-rate vs. input count-rate for three different generations of Redlen detectors. The red plots show the output count-rate for all of the 704 pixels of samples 5, 6 and 7.

The point where 100% of the detectors' pixels are non-responsive is defined as the critical flux. Figure 28 suggests that this critical flux has improved from around 1MCps.mm^{-2} (Mega count per second per mm^2) in first generation detectors to <10 MCps.mm^{-2} in second generation and >>10s of MCps.mm^{-2} in third generation, which indicates the ability of the later generations to work under the higher input X-ray fluxes.

In Figure 29 the effect of bias voltage on critical fluxes of detectors from different generations are shown. As it is expected, with the increase of the bias voltage, the drift velocity of carriers increases. This makes them less probable of being trapped in the trapping centers, enabling the detectors to work in higher input fluxes. This behaviour is consistent in all three generations of detectors but the value of the critical input flux they

could operate with in a certain bias voltage was greater in third generation detectors, rather than the two other generations.

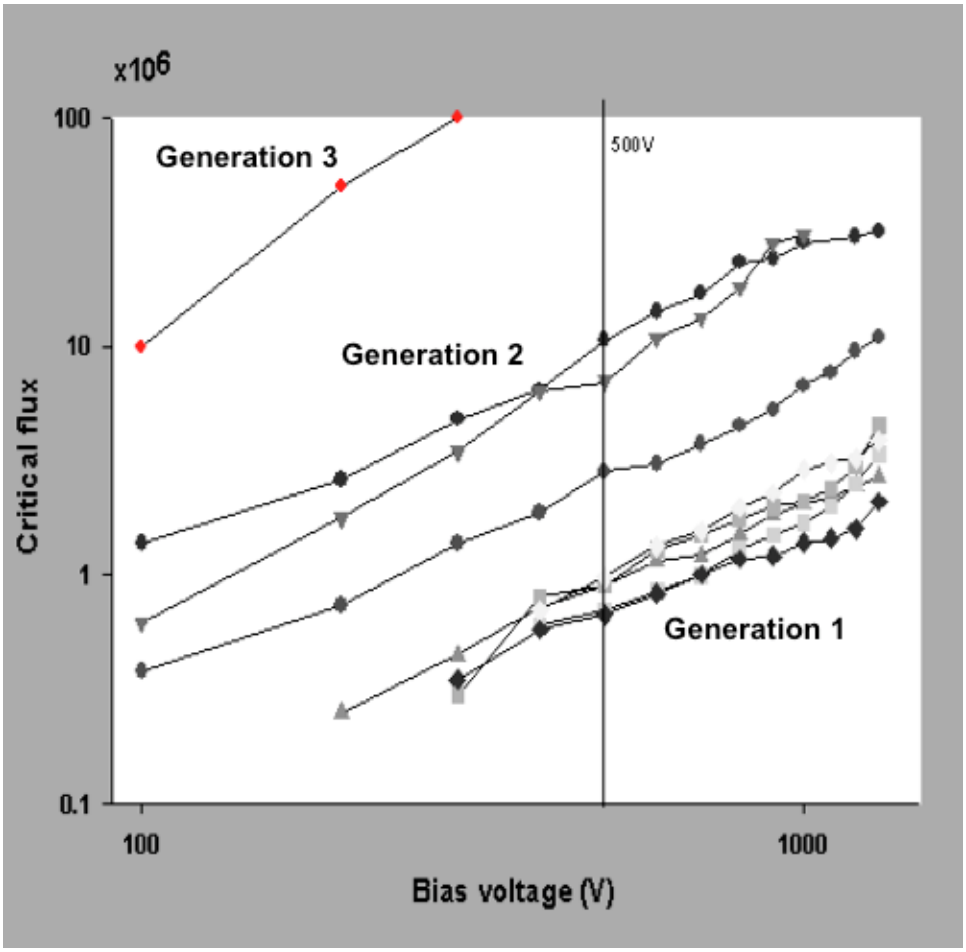

Figure 29 - Critical flux vs. bias voltage for different generations of Redlen radiation detectors. Critical flux of the later generations is noticeably higher and also it can be noted that by increasing the bias voltage, critical flux for detectors of one generation increase.

4.2.2 Pockels measurements on three generations of Redlen detectors

The electric field distribution in detectors five and seven from first and third generations was also investigated. These measurements were done by the help of my colleague Georgios Prekas in Redlen Technologies. Figure 30 shows the field distribution in these two detectors in dark condition and under X-ray illumination under 600V of bias voltage.

The horizontal axis represents the depth of detectors with x=0 representing the anode and x=2mm indicating the cathode.

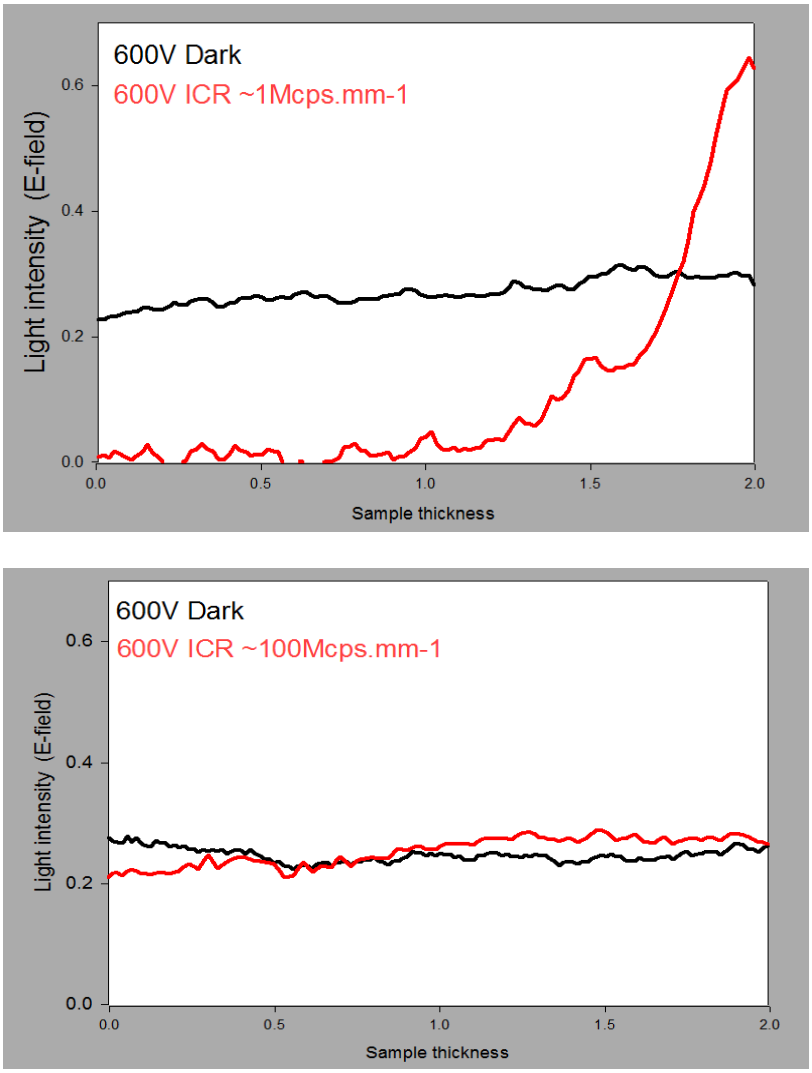

Figure 30 - Electric field distribution in the detector number five from the first generation detectors (above) and detector number seven from the third (bottom). Zero on the horizontal axis represents the anode and x=2mm is the cathode position. In first generation detectors electric field would lose its' uniformity under X-ray illumination and most of the field will drop within the first quarter of the detector thickness. Electric field in the new generation detectors on the other hand, remains uniform even after the illumination of X-ray.

As the figures suggest in the first generation detector the electric field after illumination is distorted in a way that most of the field is across the limited area close to cathode because

of polarization and almost no field is remained for the rest of the detector, resulting in problems in carriers' transfer and therefore getting no output signal. In the third generation detector, this problem is solved by precise control of the dopants in the crystal growth step and also modifying the crystal growth process to have a more uniform distribution of heat and dopants over the wafers. The Pockels measurements show a uniform electric field distribution after radiation across the whole detector thickness just as before radiation.

4.2.3 Effect of input X-ray flux and biasing voltage on the detectors' performance

Similar to the experiment performed with detectors with extended defects, effect of bias voltage and input X-ray flux were tested on polarizing detectors too. In order to do so, we used the same detectors from the first and third generations of Redlen detectors (detectors number five and seven) and measured them in a range of bias voltages and input X-ray fluxes. The results are summarized in Figures 31 and 32, respectively.

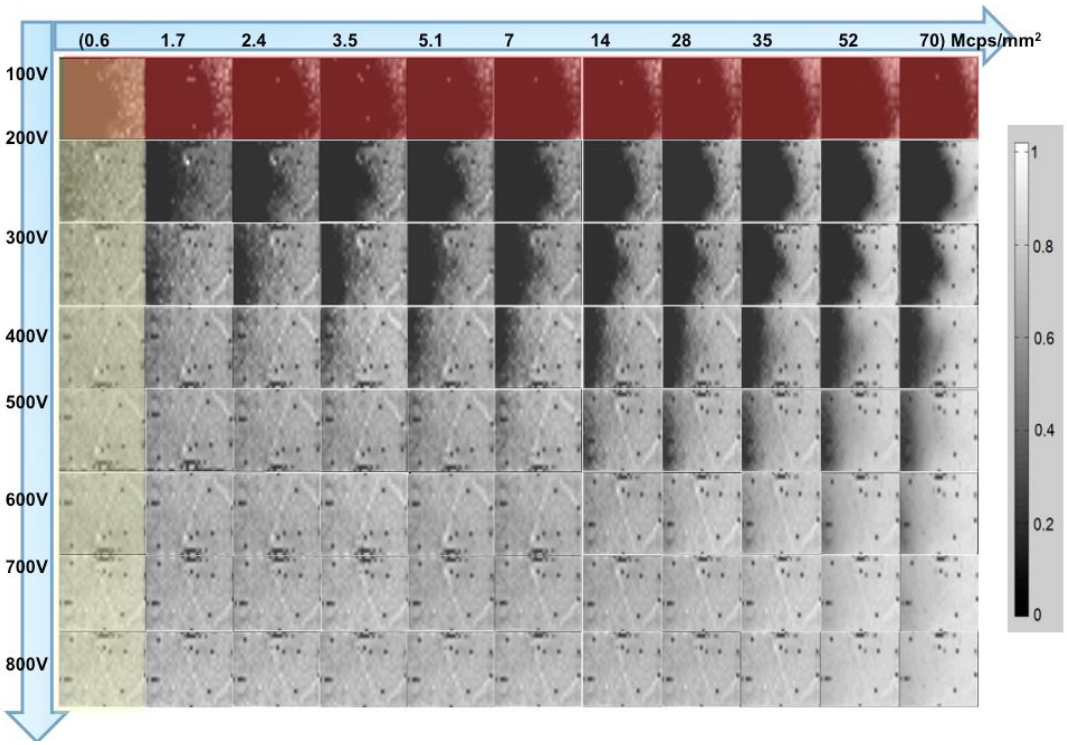

Figure 31 - Performance of detector number 5 from first generation of Redlen detectors under different X-ray fluxes (0.6-70 MCps/mm^2) and bias voltages (100-800V). It can be noticed that by increasing the flux in a constant voltage the surface of the dead area increases. It shows in a constant voltage by introducing more photons to a material with active traps, more of them will be trapped and hence we get more of the dead areas. On the other hand by having a constant input flux and increasing the bias voltage carriers' velocity increases and they will get less trapped in the trapping centers and the dead areas will restore.

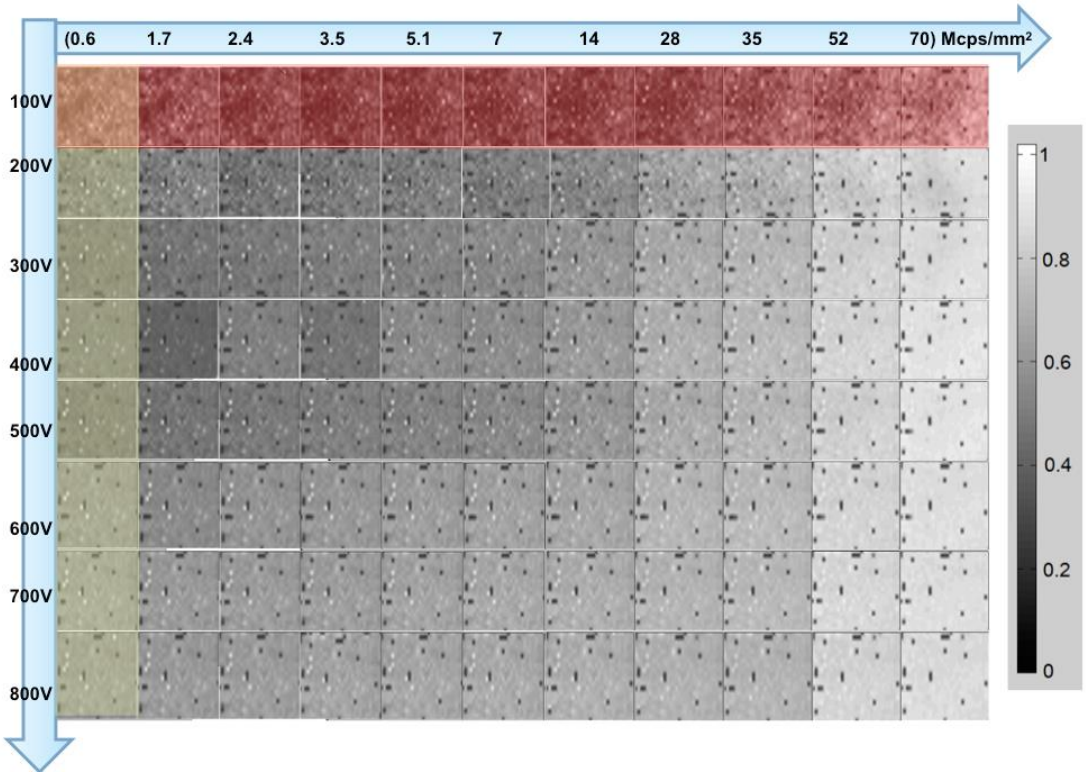

Figure 32 - Performance of detector number 7 from third generation of Redlen detectors under different X-ray fluxes and bias voltages. The detector shows a uniform result even with low bias voltages and under high input X-ray fluxes.

As the figures clearly suggests, the dead region of the detector number five with poor performance increased by increasing the input flux under a constant voltage, which happens due to higher number of photons getting trapped in the present trap centers in the material, but moving in a column towards higher bias voltages leads it to restore its good performance. The second detector, detector number seven, has a uniform performance even in low bias voltages and with high input fluxes. This detector suggests a promising good, non-polarizing performance even under high input fluxes of X-ray radiation.

4.2.5 Instability of third generation detectors

In this experiment, high bias voltage of 700V was applied to detector number eleven from third generation of Redlen detectors over a long period of time (six hours) with no X-ray irradiation. After every two hours the X-ray was applied and the performance of the detector was evaluated. In Figure 33, performance of the detector over this period of the time is shown.

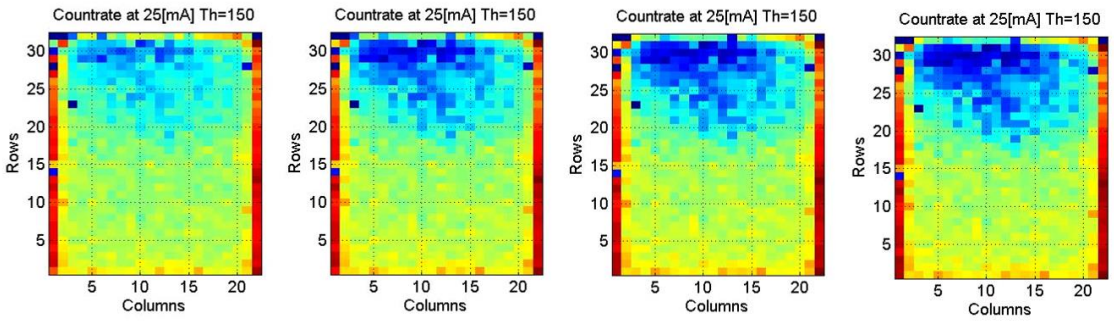

Figure 33 - Detector number eleven after being kept under 700V bias without X-ray radiation, measured in t=0, 2h, 4h and 6h. Performance degradation of the detector with time is noticeable.

Degradation of the detector's performance can be clearly seen. This instability over time is believed to happen because of point defects present in the material.

To investigate this phenomenon in more details, behaviour of three pixels from areas with good, medium and bad performance of the same detector were monitored. In Figures 34, 35 and 36, the behaviour of the pixels after staying under bias and without X-ray radiation is shown in every two hours and then applying the X-ray to evaluate the performance over a total time course of six hours.

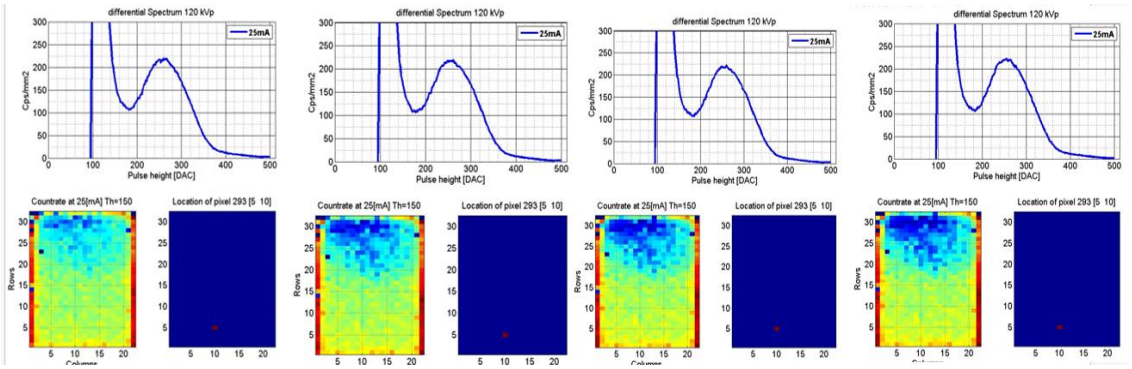

Figure 34 - Output spectra of a good pixel of detector number eleven after staying under constant bias and no irradiation for 2h periods and then applying the X-ray to examine the OCR map and spectrum over a total time course of 6h.

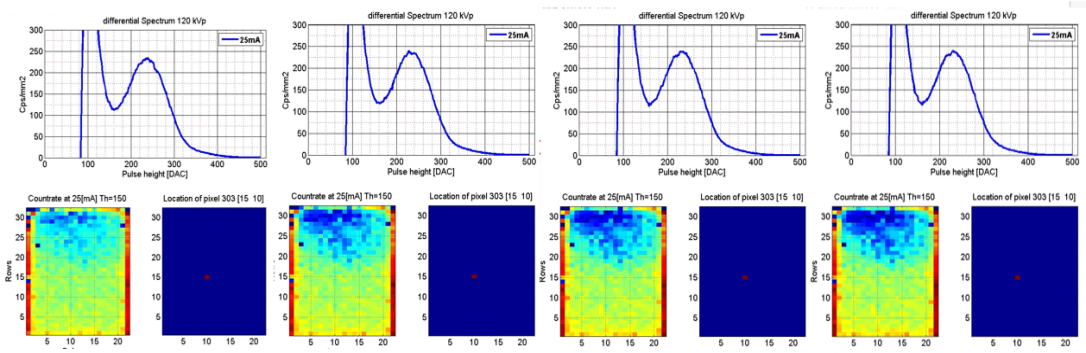

Figure 35 - Output spectra of a medium pixel of detector number eleven after staying under constant bias and no irradiation for 2h periods and then applying the X-ray to examine the OCR map and spectrum over a total time course of 6h.

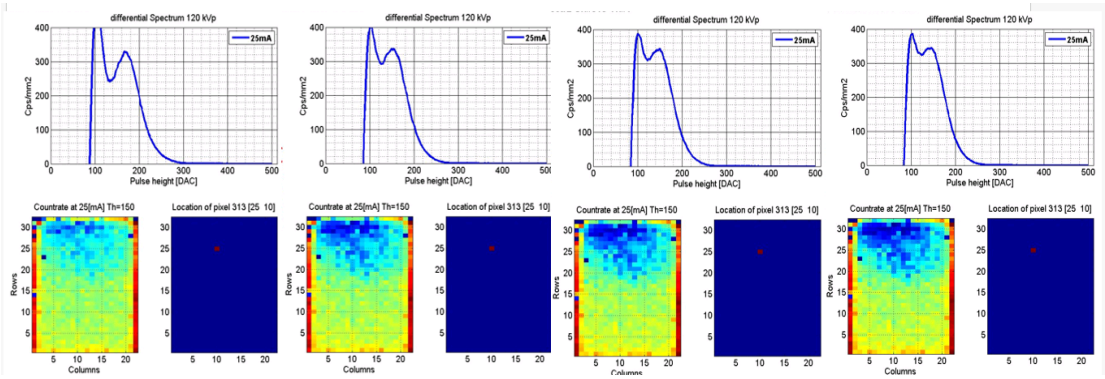

Figure 36 - Output spectra of a bad pixel of detector number eleven after staying under constant bias and no irradiation for 2h periods and then applying the X-ray to examine the OCR map and spectrum over a total time course of 6h.

As it is suggested by the figures, the spectrum of the pixel from the area with good performance shows stability over time and the performance doesn't degrade severely. For

the medium pixel the spectra has shifted to the left very slightly, but it is still stable over time, whereas in the case of the bad pixel, with increasing the time the peak in spectra moves noticeably to the left and after six hours it can be seen that polarization is strong and the pixel has almost failed to detect the X-ray.

4.2.6 DLTS measurements for third generation of Redlen detectors

In this step, three samples with different performance qualities from the third generation of Redlen detectors were measured with DLTS. In Figure 37 the results of these measurements are presented. Sample number eight showed uniform performance under different voltages, some polarization effect was observed for sample number nine and sample number ten was completely polarized for low bias voltages.

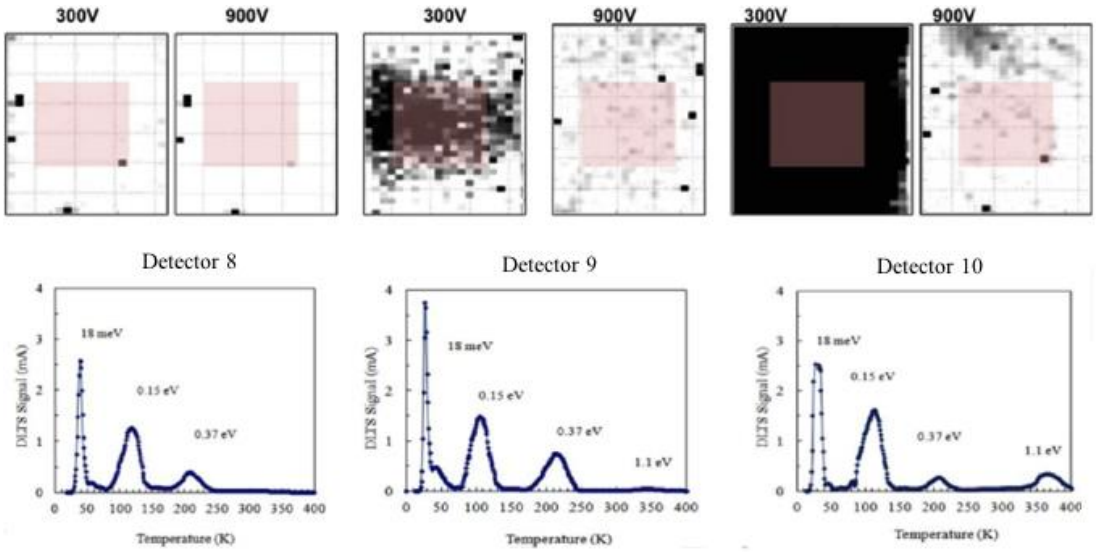

Figure 37 - X-ray count-rate maps of detectors number eight, nine and ten on the top and their DLTS plots on the bottom. Each peak represents the energy level of a trap center in the material. As the figures suggest trap level 1.1 eV has direct relationship with the polarization of the third generation detectors.

It is shown in the results that these samples also have some shallow energy defects at 18meV, 0.15eV and 0.37eV, but the defect that seems to be directly related to the performance of these detectors is 1.1eV energy level trap.

Here we can use Tables 2 and 3 from the theory section to understand the source of these point defects. Shallow defects in these detectors can be related to the Indium impurities (15-25meV) introduced to the material during growth to achieve higher resistivity and Cd vacancies (0.14-0.18eV and 0.32-0.38eV) occurred also during the crystal growth. Unfortunately the source for 1.1eV traps, which seems to be the variable directly related to the performance of the unstable detectors, is still a matter of debate. Different claims have been made regarding the source of this energy level trap. Te vacancies occurring during the growth process is one of the possible sources this trap introduced by a number of studies. [77,79,81] Dislocations of the crystal have also been introduced as another possible source. [80] Ongoing research about this deep level defect is being conducted to identify the reasons of its occurrence and eliminate it to improve the stability of the detectors. [76-81]

4.2.7 CoReMa mapping versus EPD mapping

The same experiment performed in section 4.1.4 was done on wafer number two. CoReMa and EPD maps of the wafer was recorded and the results were very interesting, due to the fact that this time not only they were recognizing extended defects in the wafer, but also showing the effects of point defects on the resistivity. In Figure 38 you can see the CoReMa map of wafer number two versus its EPD map.

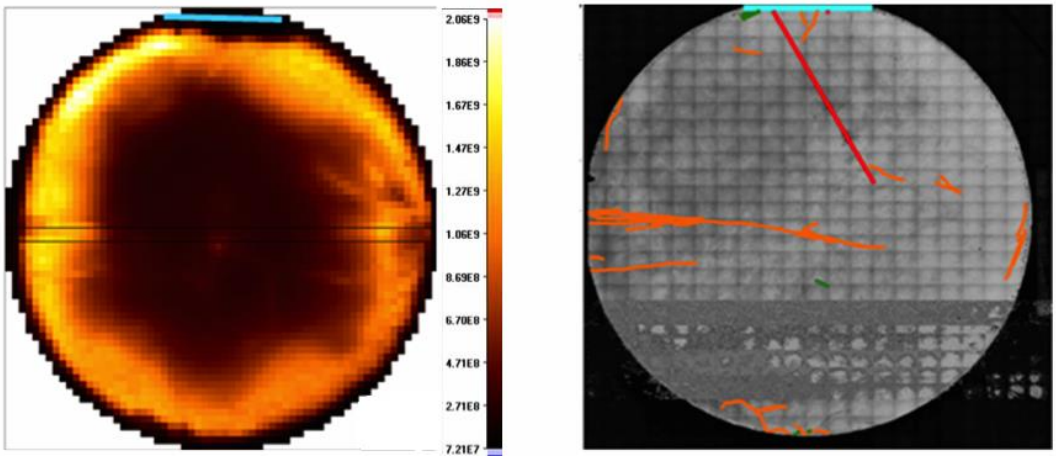

Figure 38 - CoReMa map of wafer number two versus its EPD map. Edges in CoReMa map show high resistivity area, which is explained by the presence of deep energy level traps. The twin and sub-grain boundaries shown in EPD map are covered by the low resistivity area in CoReMa map.

As suggested by the figures, the second wafer does not show uniform resistivity in the CoReMa mapping. The results suggest that the high resistivity donut shape of the wafer can be explained by the presence of point defects with an energy level lower than the Fermi level, increasing the resistivity in those areas and altering the performance of the material. This deep level trap is suggested to be the same 1.1eV energy level trap proved to cause the instability in the detectors. Also a twin boundary on the EPD map of the wafer is traceable, which cannot be distinguished in the CoReMa map as it is masked by the low resistivity area.

4.3 Discussion

4.3.1 Performance of detectors with extended defects

As we saw in the experiments performed in section 4.1 extended defects can degrade the performance of the CZT detectors severely. Two main problems caused by these defects are charge steering and charge channelling.

- **Charge steering:** As shown in Figures 19, 21 and 24, the star shaped defects and mosaics have caused dark (cold) regions in the output of the OCR maps, which represents the charge steering in the detectors. These defects act as blocks on the way of travelling carriers, causing lateral polarization and steering of the carriers and leaving the area as a low output count-rate area in the final map.
- **Charge channelling:** Another important problem caused by extended defects is charge channelling seen in Figures 21, 23, 25 and 26. The twins, sub-grain boundaries and dislocation lines present in these Figures are usually decorated with low resistivity Te inclusions, which attract charge carriers toward them causing higher number of output counts in the OCR maps, which are referred as hotlines. These areas could also be easily seen in the CoReMa maps due to their low resistivity.
- **Effect of input X-ray flux and bias voltage:** We also studied the effect of input X-ray flux and voltage on the disturbed areas of the output due to the extended defects. (Figures 23 and 24) It was demonstrated that increasing the input X-ray flux doesn't help the effect of extended defects on the OCR map, but increasing the bias voltage can improve the performance of the detectors with extended defects and the detectors are restored after a certain voltage. This can be explained by the increasing electric field over the detector, help carriers have higher drift velocity and thus better transport of them.

4.3.2 Performance of detectors with point defects

Performance of detectors with point defects was examined in section 4.2. Two major phenomena happen in detectors with high number of point defects. One of them is X-ray

induced polarization and the other one is bias induced polarization. Both types were observed and will be discussed in the following sections.

- **X-ray induced polarization:** Three generations of Redlen detectors in terms of polarization and critical flux were compared. The output count-rate versus input count-rate graph (Figure 28) of detectors from different generations was showing the degradation of detectors' performance after exposing to higher input X-ray fluxes in earlier generations of Redlen detectors. This was explained by polarization in the early generation detectors. Due to high number of hole traps in those detectors, after generating a high number of excess carriers by X-ray radiation the slower holes were trapped, causing non-uniform distribution of electric field. This would affect the drift velocity of the carriers and make the sensing process sensitive to the position of electron-hole pair generated. The electron-hole pairs generated further than the limited area close to cathode, which had the greatest portion of electric field, could not travel far and be sensed through the contacts. The electric field distribution in those detectors before and after X-ray radiation is shown in Figure 30.

  On the next step the effects of input X-ray flux and bias voltage on the performance of the first generation detectors with hole traps causing polarization and third generation with no hole traps were investigated. The results are shown in Figures 31 and 32. As expected, by increasing the input flux polarization effect in first generation detectors increases, as more excess carriers are injected into the material. Increasing biasing voltage on the other hand, increases the electric field intensity and therefore the carriers drift velocity, helping them to be less trapped. In high bias voltages, around 900V, the polarizing detectors are

completely restored. Third generation detectors on the other hand, show a uniform performance over different range of biasing voltages and input fluxes.

As it can be concluded from the above results, the problem of hole traps is solved in the new generations of radiation detectors with modifying the growth process and carefully adding the dopants during this process and is no longer a major problem in Redlen detectors.

- **Bias induced polarization:** Although the problem of hole traps has been solved for the newer generations of Redlen detectors, they still suffer from another type of polarization, which occurs even before applying the X-ray radiation. As discussed in the theory chapter, deep donor traps, which are normally occupied in the bulk of CZT material, might get empty and activated due to the band bending close to the metal-semiconductor interface. As the depletion region of this interface changes by time, the number of activated trapping centers also change and cause the instability of the detectors over time. In Figure 33 this time-dependant behaviour is shown. The detector was under bias without any X-ray illumination for six hours and after every two hours the performance of it was examined. Figures 34, 35 and 36 show the behaviour of three pixels of the same detector from regions with different qualities over time. The pixel from the good quality area shows a stable output over time, where the pixel from the area with low output count-rate shows a very unstable behaviour over time, almost failing after six hours under bias.

  To prove the existence of deep energy level traps, DLTS measurements were performed again. The results in Figure 37 show the presence of a donor trap with 1.1eV energy level. The source of this trap is still under debate. Te vacancies

occurring during growth process or dislocations within the crystal have been suggested as the possible sources of this trap in different studies. [82-85] Results of CoReMa mapping, showing high resistivity of the donut shaped edge of the unstable wafers, also agree with presence of deep level traps proved to be effective on instability of the detectors.

5 Conclusion

We studied the presence of the extended and point defects and their effect on the degradation of X-ray detectors' performance using in-house measurement instruments such as high flux tester as well as other methods like IR imaging, EPD mapping, Pockels measurements, DLTS and CoReMa. Comparison between the results of these techniques and the performance of the detectors confirmed the direct relationship between the presence of the extended defects and degradation in detectors' performance.

Detectors with point defects would suggest two types of polarization. The results from first group of detectors, which belonged to older generations of Redlen detectors, suggested that by applying high fluxes of input X-ray the holes would get trapped very close to where they were generated (on the cathode side) and the output count-rate would lose its linearity with respect to input count-rate. The results of Pockels measurements also approved the non-uniform distribution of electric field close to the cathode. The problem of hole trapping was later solved by modifying the growth process and accurate control of dopants during the growth.

The other case in which polarization phenomenon was observed was when the detectors were under high bias voltages over long periods of time. The results were showing the expansion of dead regions in the output over time and under bias, without any input X-ray flux. The DLTS measurements for these samples suggested the presence of deep level electron traps being activated by applying bias voltage over the metal-semiconductor contacts. The source of these traps measured to have an energy of 1.1 eV are still a matter of debate.

All of these findings can be used as an important feedback to improve the crystal growth and detector fabrication process to achieve higher quality materials and better performing detectors.

In future research, more investigation on the source of 1.1eV electron traps and their behaviour under different operational conditions is suggested to improve the functionality and stability of the detectors. Also more samples from other providers can be compared to study different types of defects present in different samples. In this study only samples provided by Redlen Technologies were studied.

Bibliography

[1] James, R. B., et al. "Material properties of large-volume cadmium zinc telluride crystals and their relationship to nuclear detector performance." *Journal of electronic materials* 27.6 (1998): 788-799.

[2] Ziegler, James F. "Nuclear instruments and methods in physics research section B: Beam interactions with materials and atoms." *SRIM-2003* 219 (2004): 1027-1036.

[3] Eisen, Y., and A. Shor. "CdTe and CdZnTe materials for room-temperature X-ray and gamma ray detectors." *Journal of crystal growth* 184 (1998): 1302-1312.

[4] Knoll, Glenn F. "*Radiation detection and measurement*", Third edition John Wiley & Sons, (1989).

[5] G. I. Prekas, *"Electric field studies on Cadmium Zinc Telluride (CdZnTe) Materials"*, Diss. University of Surrey, Surrey, (2010).

[6] T.E. Schlesinger, R.B. James (Eds.), *Semiconductors for Room Temperature Nuclear Applications*, Vol. 43, Academic Press, New York, (1995): 335.

[7] Lumb, D. H., et al. "Development of compound semiconductor detectors at ESA." *Nuclear Instruments and Methods in Physics Research Section A: Accelerators, Spectrometers, Detectors and Associated Equipment* 568.1 (2006): 427-432.

[8] Eisen, Y., A. Shor, and I. Mardor. "CdTe and CdZnTe gamma ray detectors for medical and industrial imaging systems." *Nuclear Instruments and Methods in Physics Research Section A: Accelerators, Spectrometers, Detectors and Associated Equipment* 428.1 (1999): 158-170.

[9] Schlesinger T E, Toey J E, Yoon H, Lee E Y, Brunett B A, Franks L and James R B, "Cadmium zinc telluride and its use as a nuclear radiation detector material" *Mater. Sci. Eng. R* 32 (2001): 103-189.

[10] Luke, P. N., and E. E. Eissler. "Performance of CdZnTe coplanar-grid gamma-ray detectors." *IEEE Transactions on Nuclear science* 43.3 (1996): 1481-1486.

[11] Bolotnikov, A. E., et al. "Factors limiting the performance of CdZnTe detectors." *Nuclear Science, IEEE Transactions on* 52.3 (2005): 589-598.

[12] K. G. Lynn, M. Weber, H. L. Glass, J. P. Flint, and Cs. Szeles, "Improved CdZnTe detectors grown by Bridgman process," *Mater. Res. Soc. Symp. Proc.* 487 (1998): 229.

[13] Maiti, C. K., L. K. Bera, and S. Chattopadhyay. "Strained-Si heterostructure field effect transistors." *Semiconductor science and technology* 13.11 (1998): 1225.

[14] Babalola, Oluseyi Stephen. *Surface and bulk defects in cadmium zinc telluride and cadmium manganese telluride crystals*. Diss. Vanderbilt University, (2009).

[15] Wilcox, William R. "Crystal Growth Technology", John Wiley & Sons, (2004): 639-639.

[16] K. Zanio, Willardson, Beer, Teatise (Eds.), *Cadmium Telluride, Semiconductors and Semimetals*, Vol. 13, Academic Press, San Diego, (1978): 53.

[17] N. Peyghambarian, S.W. Koch, and A. Msyrowicz, *"Introduction to Semiconductor Optics"*, Prentice-Hall, Englewood Cliffs, (1993).

[18] Pandy, Arun, et al. "Analysis of the growth of cadmium zinc telluride in an electrodynamic gradient freeze furnace via a self-consistent, multi-scale numerical model." *Journal of crystal growth* 276.1 (2005): 133-147.

[19] Li, Tiesheng, H. J. Lozykowski, and John L. Reno. "Optical properties of CdTe/Cd 1− x Zn x Te strained-layer single quantum wells." *Physical Review B* 46.11 (1992): 6961.

[20] M. Chu, S. Terterian, D. Ting, R. B. James, M. Szawlowski, and G. J. Visser, "Effects of p/n inhomogeneity on CdZnTe radiation detectors," *SPIE Proc. Ser.*, vol. 4784, (2003): 237-243.

[21] Li, Guoqiang, et al. "Impurities in CdZnTe crystal grown by vertical Bridgman method." *Nuclear Instruments and Methods in Physics Research Section A: Accelerators, Spectrometers, Detectors and Associated Equipment* 534.3 (2004): 511-517.

[22] Triboulet, R., and G. Neu. "Growth in one operation of the (Cd, Hg) Te alloys of all compositions to study the alloy disorder." *Journal of Crystal Growth* 72.1 (1985): 258-263.

[23] Szeles, Csaba, and Elgin E. Eissler. "Current issues of high-pressure Bridgman growth of semi-insulating CdZnTe." *MRS Proceedings*. Vol. 484. Cambridge University Press, (1997).

[24] Raiskin, E., and J. F. Butler. "CdTe low level gamma detectors based on a new crystal growth method." *Nuclear Science, IEEE Transactions on* 35.1 (1988): 81-84.

[25] Doty, F. P., et al. "Properties of CdZnTe crystals grown by a high pressure Bridgman method." *Journal of vacuum Science & technology B* 10.4 (1992): 1418-1422.

[26] V.T. Komar, Technical Report, *National Academy of Sciences of the Ukraine*, Department of Optical and Constructional Crystals, Kharkov, Ukraine, (1997).

[27] Szczerbakow, A., et al. "Structural defects and compositional uniformity in CdTe and Cd 1− x Zn x Te crystals grown by a vapour transport technique." *Journal of crystal growth* 191.4 (1998): 673-678.

[28] Ben-Dor, L., and N. Yellin. "Vertical unseeded vapor growth and characterization of Cd 0.95 Zn 0.05 Te crystals." *Journal of crystal growth* 71.3 (1985): 519-524.

[29] Palosz, W., S. L. Lehoczky, and F. R. Szofran. "Thermochemical model of physical vapor transport of cadmium-zinc telluride." *Journal of crystal growth* 148.1 (1995): 49-55.

[30] Melnikov, A. A., et al. "Growth of CdZnTe single crystals for radiation detectors." *Journal of crystal growth* 197.3 (1999): 666-669.

[31] Chen, Henry, et al. "Characterization of Traveling Heater Method (THM) Grown Cd 0.9 Zn 0.1 Te Crystals." *Nuclear Science, IEEE Transactions on* 54.4 (2007): 811-816.

[32] Cheuvart, P., et al. "CdTe and CdZnTe crystal growth by horizontal Bridgman technique." *Journal of crystal growth* 101.1 (1990): 270-274.

[33] Bruder, M., et al. "Vertical Bridgman growth of Cd 1− y Zn y Te and characterization of substrates for use in Hg 1− x Cd x Te liquids phase epitaxy." *Journal of crystal growth* 101.1 (1990): 266-269.

[34] Glass, H. L., et al. "Improvements in production of CdZnTe crystals grown by the Bridgman method." *Journal of crystal growth* 184 (1998): 1035-1038.

[35] Lauer, R. B., and Ferd Williams. "Photoelectronic Properties of Graded Composition Crystals of II- VI Semiconductors." *Journal of Applied Physics* 42.7 (1971): 2904-2910.

[36] Streetman, Ben G., and Sanjay Banerjee. *Solid state electronic devices*. Vol. 4. New Jersey: Prentice Hall, (2000).

[37] Cottingham, W. N., and D. A. Greenwood. *Introduction to nuclear physics*. Cambridge, (2002):7-32.

[38] He, Zhong. "Review of the Shockley–Ramo theorem and its application in semiconductor gamma-ray detectors." *Nuclear Instruments and Methods in Physics Research Section A: Accelerators, Spectrometers, Detectors and Associated Equipment* 463.1 (2001): 250-267.

[39] Ramo, Simon. "Currents induced by electron motion." *Proc. Ire* 27.9 (1939): 584-585.

[40] M. A. Abdalla, "*Pixel detectors and electronics for high energy radiation imaging"*, Diss, The Royal institute of Technology, Stockholm, (2001).

[41] Dierickx, Bart, et al. "Color X-ray photon counting image sensing." *IISW, Hakodate Japan* 1 (2011).

[42] Schroder, Dieter K. *Semiconductor material and device characterization*. John Wiley & Sons, (2006), Chapter 5.

[43] Dierickx, Bart, et al. "Color X-ray photon counting image sensing." *IISW, Hakodate Japan* 1, (2011).

[44] Yang, Ge, et al. "Effects of In doping on the properties of CdZnTe single crystals." *Journal of crystal growth* 283.3 (2005): 431-437.

[45] Hage-Ali, Makram, and Paul Siffert. "Growth Methods of CdTe Nuclear." *Semiconductors for room temperature nuclear detector applications* 43 (1995): 219.

[46] Bastard, Gerald, and Helmut Oppolzer, eds. *Analytical techniques for the characterization of compound semiconductors*. Elsevier, (1991).

[47] Wald, F. V. "Applications of CdTe. A review." *Revue de Physique Appliquée* 12.2 (1977): 277-290.

[48] Siffert, P., et al. "Cadmium telluride nuclear radiation detectors." *Nuclear Science, IEEE Transactions on* 22.1 (1975): 211-225.

[49] Scharager, C., et al. "Determination of deep levels in semi-insulating cadmium telluride by thermally stimulated current measurements." *physica status solidi (a)* 31.1 (1975): 247-253.

[50] E.E. Haller, in: P.Y. Yu, M. Carlona (Eds.), *Fundamentals of Semiconductors*, Springer Verlag, New York, (1996): 539-541.

[51] Lee, E. Y., et al. "Compensation and trapping in CdZnTe radiation detectors studied by thermoelectric emission spectroscopy, thermally stimulated conductivity, and current-voltage measurements." *Journal of electronic materials* 28.6 (1999): 766-773.

[52] Raiskin, E., and J. F. Butler. "CdTe low level gamma detectors based on a new crystal growth method." *Nuclear Science, IEEE Transactions on* 35.1 (1988): 81-84.

[53] Chern, S. S., H. R. Vydyanath, and F. A. Kro. "The defect structure of CdTe: Hall data." *Journal of solid state chemistry* 14.1 (1975): 33-43.

[54] Culity, B. D., and S. R. Stock. "Elements of X-ray Diffraction." *Reading: Addition-Wesley* (1978).

[55] Everson, W. J., et al. "Etch pit characterization of CdTe and CdZnTe substrates for use in mercury cadmium telluride epitaxy." *Journal of electronic materials* 24.5 (1995): 505-510.

[56] Zha, Gangqiang, et al. "Study of dislocations in CdZnTe single crystals." *physica status solidi (a)* 204.7 (2007): 2196-2200.

[57] Ralph W. G. Wyckoff, “Crystal Structures 2nd edition”., Interscience Publisher, New

York, (1963).

[58] Rudolph, P. "Non-stoichiometry related defects at the melt growth of semiconductor compound crystals–a review." *Crystal Research and Technology* 38.7-8 (2003): 542-554.

[59] Yang, G., et al. "'Star- like'defects in Cd- annealed CdZnTe crystals—an experimental study of their origin and formation mechanism." *Crystal Research and Technology* 48.4 (2013): 221-226.

[60] Koyama, A., A. Hichiwa, and R. Hirano. "Recent progress in CdZnTe crystals." *Journal of electronic materials* 28.6 (1999): 683-687.

[61] Garg, Arun Kumar, et al. "Improvement in crystalline quality of Cd 1− x Zn x Te (x= 4%) crystals grown in graphite crucible." *Journal of crystal growth* 260.1 (2004): 148-158.

[62] Ray, A. K., et al. "Precision of light scattering techniques for measuring optical parameters of microspheres." *Applied optics* 30.27 (1991): 3974-3983.

[63] Malm, H. L., and M. Martini. "Polarization phenomena in CdTe nuclear radiation detectors." *Nuclear Science, IEEE Transactions on* 21.1 (1974): 322-330.

[64] Siffert, P., et al. "Polarization in cadmium telluride nuclear radiation detectors." *Nuclear Science, IEEE Transactions on* 23.1 (1976): 159-170.

[65] Malm, H. L., et al. "Gamma− ray spectroscopy with single− carrier collection in high− resistivity semiconductors." *Applied Physics Letters* 26.6 (1975): 344-346.

[66] Hage-Ali, M., et al. "Studies of CdTe surfaces with secondary ion mass spectrometry, Rutherford backscattering and ellipsometry." *Applied physics* 19.1 (1979): 25-33.

[67] Fink, Johannes, et al. "Characterization of charge collection in CdTe and CZT using the transient current technique." *Nuclear Instruments and Methods in Physics Research Section A: Accelerators, Spectrometers, Detectors and Associated Equipment* 560.2 (2006): 435-443.

[68] Zanio, K. R., W. M. Akutagawa, and R. Kikuchi. "Transient Currents in Semi-Insulating CdTe Characteristic of Deep Traps." *Journal of Applied Physics* 39.6 (1968): 2818-2828.

[69] Butler, Jack F., et al. "Gamma and X-ray detectors manufactured from Cd1− xZnx Te grown by a high pressure bridgman method." *Materials Science and Engineering: B* 16.1 (1993): 291-295.

[70] Elhadidy, H., et al. "Study of polarization phenomena in n-type CdZnTe." *Journal of Physics D: Applied Physics* 47.5 (2014): 055104.

[71] Bolotnikov, Aleksey E., et al. "Properties of Pt Schottky type contacts on high-

resistivity CdZnTe detectors." *Nuclear Instruments and Methods in Physics Research Section A: Accelerators, Spectrometers, Detectors and Associated Equipment* 482.1 (2002): 395-407.

[72] Soldner, Stephen, Derek S. Bale, and Csaba Szeles. "Dynamic lateral polarization in CdZnTe under high flux X-ray irradiation." *Nuclear Science, IEEE Transactions on* 54.5 (2007): 1723-1727.

[73] Parker, Bradford H., et al. "Effect of twin boundaries on the spectroscopic performance of CdZnTe detectors." *International Symposium on Optical Science and Technology*. International Society for Optics and Photonics, (2001).

[74] B. Norlin, "*Characterisation and application of photon counting X-ray detector systems"*, Diss. Mid Sweden University, (2007).

[75] B.D. Guenther, *modern optics*, John Wiley and sons Inc., (1990): 191-340.

[76] Castaldini, A., et al. "Deep energy levels in CdTe and CdZnTe." *Journal of applied physics* 83.4 (1998): 2121-2126.

[77] Haddara, Hisham, ed. *Characterization methods for submicron MOSFETs*. Vol. 352. Springer Science & Business Media, (2012).

[78] Gul, R., et al. "Point defects in Pb-, Bi-, and In-doped CdZnTe detectors: deep-level transient spectroscopy (DLTS) measurements." *Journal of electronic materials* 41.3 (2012): 488-493.

[79] Lang, D. V. "Deep- level transient spectroscopy: A new method to characterize traps in semiconductors." *Journal of applied physics* 45.7 (1974): 3023-3032.

[80] Li, Qiang. *The Influence of Stoichiometry on Electrical Properties of Silicon Carbide Grown by Physical Vapor Transport Process*. ProQuest, (2005).

[81] Donecker, J., S. Rautenstrauch, and S. Bergmann. "Quick EPD mapping of GaAs." *Conference Series-Institute of ohysics*. Vol. 160. IOP publishing LTD, (1998).

[82] Castaldini, A., et al. "Deep energy levels in CdTe and CdZnTe." *Journal of applied physics* 83.4 (1998): 2121-2126.

[83] Drighil, A., et al. "Properties of Cd1-xZnxTe crystals grown by High Pressure Bridgman (HPB)." *MJ Condensed Matter* 2 (1999): 54-57.

[84] Kim, K. H., et al. "New insight into the 1.1-eV trap level in CdTe-based semiconductor." *Journal of the Korean Physical Society* 62.4 (2013): 623-627.

[85] Rodríguez-Fernández, J., et al. "Relationship between the cathodoluminescence

emission and resistivity in In doped CdZnTe crystals." *Journal of Applied Physics* 106.4 (2009): 044901.